2004

Acoustical and flow characteristics of a cough as an index of pulmonary function in the guinea pig

Joshua W. Day
West Virginia University

Acoustical and Flow Characteristics of a Cough as an Index of Pulmonary Function in the Guinea Pig

Joshua W. Day

Thesis Submitted to the College of Engineering and Mineral Resources at West Virginia University in partial fulfillment of the Requirements for the degree of

Master of Science
in
Electrical Engineering

Mark Jerabek, Ph.D., Co-chair
Dave Frazer, Ph.D., Co-chair
Wils Cooley, Ph.D.

Department of Computer Science and Electrical Engineering

Morgantown, West Virginia
2004

Keywords: Cough, Guinea pig, Airway Resistance

ABSTRACT

Acoustical and Flow Characteristics of a Cough as an Index of Pulmonary Function in the Guinea Pig

Joshua W. Day

Human studies have shown that cough sound and flow analysis may be useful for diagnosing pulmonary abnormalities. The purpose of this study was to evaluate an animal model for cough sound and flow analysis. A system was designed to expose guinea pigs to aerosols of citric acid (0.39M) and record resulting coughs at different stages of chemically induced specific airway resistance (sR_{AW}). sR_{AW} changes were determined by comparing the phase differences in the nasal and thorax flows during breathing cycles using dual chamber plethysmography. Coughs were divided into three categories (low sR_{AW}, n=113; moderate sR_{AW}, n=143; high sR_{AW}, n=93). 124 cough sound parameters were derived from the analysis of the sound pressure waves recorded during the cough. The signal analysis included filter octave analysis, frequency power analysis, and time dependent spectral analysis. Unacceptable coughs were defined as those having 10% or more parameters exceeding two standard deviations from the mean and were eliminated from each group. A principal component analysis was performed on all of the data, and components describing 99% of the variability in the parameters were chosen to train a single neuron feed-forward back propagation neural network with a bipolar sigmoid output transfer function. The classification system was able to correctly discriminate between members of the high and low airway constriction groups with an accuracy of 0.946 and a sensitivity and specificity of 0.893.

Acknowledgements

I would like to thank Dr. David Frazer for his guidance and expertise throughout my thesis work, and I would like to thank my committee members, Dr. Wils Cooley and Dr. Mark Jerabek, for their advice and constructive comments along the way. I would like to thank Jeff Reynolds and the rest of the Developmental Engineering Research Team of NIOSH for the knowledge and support they provided over the course of this research. I would also like to thank Amy Frazer and Michelle Donlin for all their help in carrying out the exposures.

I would like to express my sincere gratitude to the people in my life that have helped and supported me throughout my entire graduate career. I would like to thank my wife, Jamie Day, for her patience, understanding, encouragement, and the love and friendship we share. I would also like to thank my parents, Joe and Joy Day, for all of their prayers, guidance, and undying support as I pursued my dreams. I would like to thank my brother, Jeremy Day, for being my canoe partner and fishing buddy when I needed a break from it all. I would like to thank my wife's parents, Carlton and Barbara Jones, for their encouragement and faith in me. I would also like to thank my friend, Scott Day, for his valued advice and continued support.

Most of all, I would like to give thanks to God for being with me during this and all of life's triumphs and difficulties. With Him all things are possible.

Table of Contents

List of Figures

List of Tables

Chapter 1 - Introduction

Cough is a natural respiratory defense mechanism and one of the most common symptoms of respiratory disease [1]. It is often the foremost indicator of many fatal diseases. The United States alone spends nearly $600 million annually on over-the-counter cough and prescription medications for cough [30]. In a United Kingdom primary care report, approximately four and a half million consultations per year claimed cough to be their main complaint [2]. This ranks cough fifth in the most common disorders for which patients seek medical advice, constituting a total of 30 million office visits per year in the US [28].

There is a need for quickly and accurately diagnosing potential pulmonary disease in patients suffering from cough. Many cough studies focus on the anatomical and physiological mechanisms responsible for cough. Since cough can be readily observed and measured in a variety of fashions, it would be beneficial to diagnose possible respiratory illness directly from cough sound and flow characteristics [3]. Many studies include measuring the number of coughs provoked by chemical aerosols to gain further insight into what triggers the cough response and airway constriction. Ongoing cough research conducted at the National Institute for Occupational Safety and Health (NIOSH) aims to characterize both the acoustical and flow properties found in the human cough [4-8]. Findings from this research indicate that it is possible to determine whether humans studied exhibit normal pulmonary function or suffer from some form of pulmonary disease. The capability of distinguishing pulmonary disorders using a cough provides a repeatable and reliable way of diagnosing respiratory illnesses.

In a variety of occupations, workers are exposed to many types of aerosol contaminants that deposit in the respiratory tract. For many occupational pollutants, the deposition of these aerosols has been studied in considerable detail. However, experiments are rarely conducted with readily available volunteers to draw immediate conclusion as to how the aerosols are affecting the respiratory tract during different levels of exposure. This is due primarily to the health risks associated with such exposures. It would be beneficial to the ongoing development of this research to use an animal model to conduct more elaborate, time-dependent, and controlled studies of the effects of occupational aerosols. Using an animal model to examine resulting coughs after an exposure to a common occupational aerosol would allow the resulting changes in pulmonary activity to be contrasted to the characteristics of a pre-exposure induced cough. By studying how changes in normal pulmonary function due to inhaled aerosols change cough characteristics, these tests may provide a correlation to the expected responses of humans and a deeper understanding of the relationship between cough characteristics and respiratory function.

1.1 Problem Statement and Thesis Objective

1.1.1 Problem Statement

In the past, guinea pigs have been used to evaluate the effectiveness of drugs in reducing their cough response to chemical agents that induce airway constriction. Most studies have primarily focused on determining the number of coughs. The airflow and acoustical characteristics of a guinea pig cough have not been studied in detail.

1.1.2 Thesis Objective

The primary objective of this work is to design and construct an exposure system that can be used to collect flow and acoustical information within a guinea pig cough. Frequency power analysis, filter octave analysis, and time dependent spectral analysis will be applied to the acoustical cough signal to derive cough sound parameters. Peak flow, average flow, total volume, and peak acceleratory flow will be calculated from the cough flow signal. The acoustical and flow parameters obtained from the cough will be used to depict changes in the acoustical and flow properties at low and high levels of chemically induced airway resistance.

Chapter 2 – Review of Relevant Literature

2.1 The Cough Reflex

Cough is predominantly a reflex characteristic triggered by a peripheral stimulation. The reflex can be broken down and generalized into five simple links: receptors, an afferent pathway, a central processor, an efferent pathway, and effectors. Lung irritant receptors, pulmonary and airway stretch receptors, and laryngeal receptors are some of the many receptors associated with the cough reflex. Receptors mediating cough are found throughout the airways at epithelial nerve endings, primarily localized at sites of bifurcation or of sudden changes in the caliber of the airways. These receptors, known as rapidly adapting receptors (RARs), are the endings of myelinated fibers of the vagus nerve [1]. In addition to these receptors, some recent studies indicate that adapting stretch receptors (SARs) and C-fiber stimulation may also be involved in the cough reflex [9,10]. The afferent pathway is composed of branches of the vagus and the glossopharyngeal nerves through which the afferent inputs from the airway receptors travel [1]. This information is then passed to a portion of the central nervous system associated with respiratory reflexes, which is thought to be located in a diffuse area of the medulla and lower pons close to the nucleus solitarius [11,12]. Upon processing the information gathered and transported from the receptors, responses from the central processor are carried to the effectors by the way of the phrenic, intercostals, lumbar and vagal nerves. The effectors are the muscles responsible for retraction and enforcement of the vocal cords, the cross-striated muscles of respiration, the smooth muscles of the respiratory

system and the glands of the respiratory tract [1]. These five links work together to process information and carry out the cough reflex.

The physical cough maneuver consists of a complex sequence of inspiratory and expiratory efforts. The first phase is a preliminary inspiration of gas usually larger than the normal breath [13]. At the end of the inspiration, the glottal adductors close, the diaphragm relaxes, expiratory muscles contract, and the gas within the lungs is compressed [14]. As the glottis reopens and an excitation of the thoracoabdominal expiratory muscles occurs, the compressed air rushes from the lungs periphery at a maximal flow rate [14,15]. In the final phase, known as the cessation phase, muscle activity minimizes and airflow decreases to zero [16].

2.2 Human Cough Research

2.2.1 Sound Generation during Cough

Physicians have used pulmonary acoustics of various respiratory maneuvers to help with the diagnosis of lung disease for many years. Although cough is often considered to be a complication more so than a diagnostic tool, cough can also be used in diagnoses [6,16]. It is important to understand the changes in cough sounds due to lung disease. Cough sound is initiated by the flow of air through the large airways of the lungs. The sound then travels through the upper respiratory tract, through the oral cavity producing a broadband frequency signal, and out through the lips. The sound that is produced provides important information regarding the sound source and the filtering effects of the airways [8]

2.2.2 Cough Sound and Flow Studies

The researchers and engineers at the National Institute for Occupational Safety and Health (NIOSH) have been successful in designing a system capable of recording high fidelity cough sound measurements. The system measures the sound pressure waves propagated through the mouth during cough. The basic construction consists of a cylindrical mouthpiece attached to a 1" diameter metal tube where a microphone is mounted inside the metal tube tangent to the inner surface. A section of 1" diameter flexible tubing is attached to the metal tube opposite the mouthpiece, and an exponential horn is mounted to the opposite end of the flexible tubing to minimize acoustical reflections.

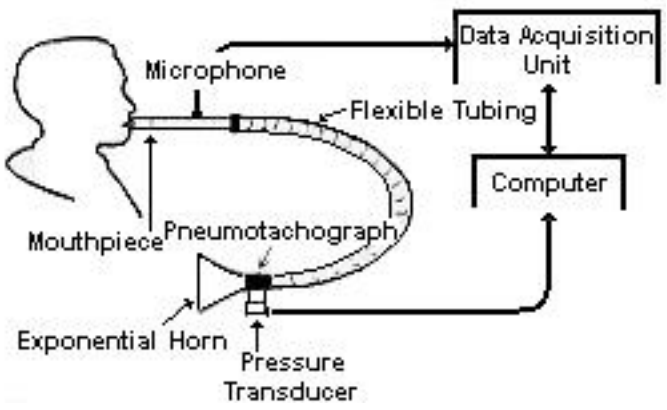

Figure 2-1 System Used to Acquire Voluntary Human Cough Sound and Flow measurements [8]

Cough sounds were digitized at 65536 Hz using a 14 bit A/D converter and saved for later analysis. The goal of the design was to have a system that can be used to examine acoustical characteristics in coughs from subjects with respiratory disease [6,8].

Upon further investigation of the digitized signals obtained from the system in Figure 2-1, distinct cough parameters were established. In one of the studies, a power spectrum created from the cough waveforms showed that the cough waveform exhibits a $1/f^{\beta}$ relationship. By using a least square analysis to apply the closest straight-line approximation of a log-log scale power spectrum, the exponent ß was approximated to be equal to the slope of the straight line. Results show that there are differences in ß between genders. This may be in part due to the differences in the caliber or arrangement of airways between men and women [8]. Another useful approach for analyzing cough waveforms is to view spectral information with respect to time. A spectrogram visually displays frequency components by plotting individual joint time-frequency color intensity blocks on a frequency versus time plot. Wheezes, continuous or slowly changing tones, are visually evident by horizontal bands of high intensity frequency components present in the spectrogram. Temporal locations, frequency levels, and duration of the wheeze can be used to characterize and diagnose different lung diseases [17].

Other studies focus on acoustic modeling theories to extrapolate information from the free field measurement of a cough sound. Many of the theories are similar to those applied in speech processing [5,18]. Van Hirtum et al used an auto-regressive acoustical model, in which the current sample, $y(t)$, is based on a finite number, n_a, of past samples

$$\hat{y}_p(t) = -\sum_{k=1}^{n_a} a_k y(t-k)$$

where $\hat{y}_p(t)$ is the predicted signal sample.

The focus of this research was to determine frequency and bandwidths of peaks in the spectra for human and animal coughs. Model order determination is discussed and the ability to depict resonances within the cough is also explained [19]. Similar models, also based on speech processing algorithms, represent the respiratory tract as a transfer function to model changing airway sizes as time varying diameter changes in lossless tubes. Findings from this research indicate that it may be possible to determine whether the cough sound can be used to reconstruct the respiratory tract areas and distinguish between healthy individuals and those with chronic pulmonary disease [5].

Cough flow characteristics have also been productive in determining differences between healthy individuals and those suffering from obstructive lung disease. Decreased peak flow, average flow, and peak acceleratory flow during cough are indicators of obstructive lung disease. It has also been shown that men and women exhibit different flow characteristics due in part to the arrangement and size of their airways, further supporting the notion that flow characteristics provide insight to actual construction of the airways [16]. By examining cough flow in conjunction with acoustical properties, the intensity and duration of the cough can more accurately be determined [7].

2.3 Guinea Pig Cough Research

Cough spectral analysis, cough sound models, and flow characteristics demonstrate great potential in obtaining distinct cough parameters in humans. Despite significant progress in human cough research, research is limited by the ability to conduct human exposures to certain occupational aerosols due to the

potential health hazards. For this reason, it is important to find an appropriate animal substitute that exhibits many of the same responses to a wide variety of aerosols. Animal studies have been conducted to estimate human pulmonary physiology for quite some time. For the validity of this research it is important to show human and guinea pig respiratory correlations. Using an animal with similar pulmonary responses to humans is the first step in creating an accurate animal cough model.

2.3.1 Occupational Irritants

In many different occupational environments, gasses, vapors, and particles can act as respiratory irritants [30]. These irritants can be classified as either sensory or pulmonary irritants. Sensory irritants stimulate the unmyelinated C-fibers of the trigeminal nerve endings located in the nasal mucosa [31,32]. In contrast, the pulmonary irritants stimulate the vagal afferents either directly or through inflammation in the conducting airways and alveoli. In guinea pigs and humans, pulmonary irritants cause a decrease in tidal volume resulting in an increase in breathing rate [20]. The effects of occupational irritants in test animals versus humans reflect correlations between pulmonary inflammation responses and evidence to the appropriate animal for this model. Table 2-1 is a collection of exposure results illustrating the amount of pulmonary inflammation to a variety of occupational irritants.

Table 2-1 Pulmonary Inflammation in Response to Inhalation of Various Gases, Vapors and Particles [20]

Agent	Exposure	Species	PMN
Cotton Dust	0	guinea pig	$0.46\pm0.04 \times 10^7$ cells/gp
	35 mg/m^3; 2h	guinea pig	$4.00\pm1.23 \times 10^7$ cells/gp
	0	rat	$0.08\pm0.01 \times 10^6$ cells/rat
	35 mg/m^3; 6h	rat	$4.47\pm1.00 \times 10^6$ cells/rat
Burnt hay	0	guinea pig	$0.10\pm0.01 \times 10^7$ cells/gp
	11 mg/m^3; 6h	guinea pig	$1.50\pm0.50 \times 10^7$ cells/gp
Chopped hay	0	guinea pig	$0.33\pm0.03 \times 10^7$ cells/gp
	6 mg/m^3; 6h	guinea pig	$2.66\pm0.60 \times 10^7$ cells/gp
Silage	0	guinea pig	$0.20\pm0.02 \times 10^7$ cells/gp
	8 mg/m^3; 6h	guinea pig	$4.33\pm0.66 \times 10^7$ cells/gp
Leaf/Wood Compost	0	guinea pig	$0.42\pm0.10 \times 10^7$ cells/gp
	30 mg/m^3; 4h	guinea pig	$5.59\pm0.84 \times 10^7$ cells/gp
Endotoxin	0	guinea pig	$0.08\pm0.03 \times 10^7$ cells/gp
	$4x10^4$ EU/m^3; 3h	guinea pig	$3.31\pm0.69 \times 10^7$ cells/gp
FMLP	0	guinea pig	$0.15\pm0.01 \times 10^7$ cells/gp
	1 mg/m^3; 4h	guinea pig	$1.38\pm0.35 \times 10^7$ cells/gp
3-Glucan	0	guinea pig	$0.30\pm0.02 \times 10^7$ cells/gp
	23 mg/m^3; 4h	guinea pig	$3.72\pm0.57 \times 10^7$ cells/gp
Leather conditioner	0	guinea pig	$0.17\pm0.06 \times 10^7$ cells/gp
	2.5 mg/m^3; 4h	guinea pig	$0.92\pm0.39 \times 10^7$ cells/gp
Asphalt fume	0	rat	$1.25\pm0.01 \times 10^6$ cells/rat
	20 mg/m^3; 4h	rat	$0.79\pm0.06 \times 10^6$ cells/rat
Ozone	0	rat	$0.40\pm0.04 \times 10^5$ cells/rat
	2ppm; 3h	rat	$3.30\pm1.10 \times 10^5$ cells/rat

In guinea pigs, the polymorphonuclear leukocytes (PMN) obtained by bronchoalveolar lavage peaks between 12 and 18 hours after the exposure. Similarly, workers exposed to these aerosols exhibited a similar time course of inflammation [20].

2.3.2 Citric Acid Cough Studies

Citric acid has been widely used to chemically induce cough in both humans and other animals [21]. The cough reflex in the rat and mouse are less documented; only chemical stimulation can induce the cough reflex, and the resulting coughs are neither reproducible nor stable [1]. In a study conducted by Tartar and Pecova, the

sensitivity of the cough reflex in laboratory animals was tested. They found that citric acid induced cough in 42.9% of unanethesized rats, 61.1% of rabbits, and 100% of the guinea pigs [22]. While examining the role of partial laryngeal denervation on the cough reflex in laboratory animals, results indicated that all guinea pigs tested, 50% of the rats, and 50% of rabbits coughed. Multiple studies by others have produced similar results confirming that guinea pigs have a more sensitive cough reflex than other laboratory animals [23].

The citric acid cough response in guinea pigs has also been proven similar to that of humans. In a comparative study of a cough challenge with humans and guinea pigs, both species exhibited similar dose dependant response curves.

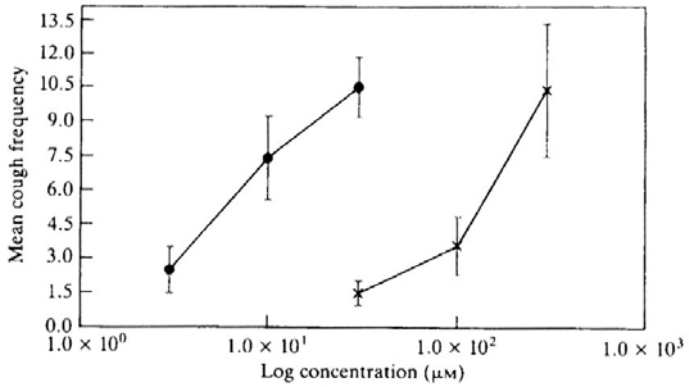

Figure 2-2 Guinea Pig Log-dose-response Curves for Citric Acid and Capsaicin [21]

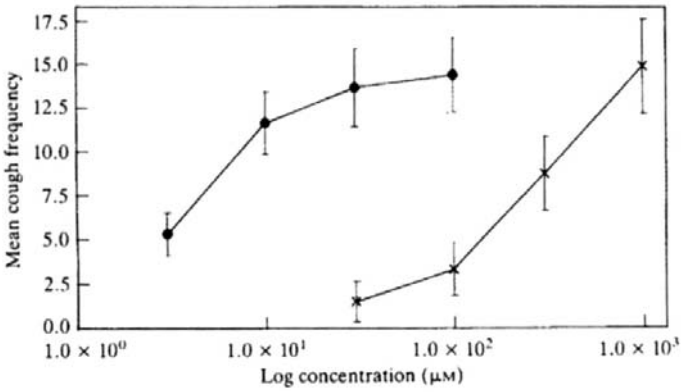

Figure 2-3 Human Log-dose-response Curves for Citric Acid and Capsaicin [21]

In Figures 2-2 and 2-3, the citric acid (-x-) and capsaicin (-●-) dose response curves are plotted for guinea pigs and humans. The points show mean (±SEM) cough frequency for each particular dose. The concentration-response relationship is comparable in both subjects [21].

2.3.3 Methods of Recording Coughs in Guinea Pigs

A variety of methods have been used to record cough in guinea pigs. In most studies, the intent was not to examine the contents of the cough sound but as a way to ensure that coughs were being counted accurately. Scientists have mainly focused their studies on the receptors and afferent pathways responsible for inducing cough using a variety of cough inducing agents [1,24,33,34]. Counting coughs accurately with a high certainty is a fundamental component in their research. Visually observing coughs proved to be subjective and provided controversial information. Using a microphone either built into the cage or attached to the animal provided a more concrete basis for counting coughs. Despite these early efforts to quantify the cough response, visual conformation of cough attempts proved essential to differentiate coughs from sneezes or growls. Other methods involved measuring changes in interpleural and tracheal pressure. This approach seemed to provide the best evaluation of quality and quantity of cough [1].

2.3.4 Cough and Bronchoconstriction

In recent studies, a common experimental protocol has been adopted for guinea pig cough challenges. Forsberg uses this protocol in a study focusing on cough and bronchoconstriction mediated by capsaicin-sensitive sensory neurons [24].

Initially, guinea pigs were placed individually in a Perspex chamber. They were then exposed to nebulized citric acid, nicotine, and capsaicin for up to 7 minutes in individual trials. Aerosols were produced by an ultrasonic nebulizer at a rate of 0.5mL/min, and two trained observers watched the animals and listened to amplified sounds in order to accurately denote coughs. The two observers reported 0.39M citric acid produced 6±3 and 5.8±3 coughs respectively in the first 3 minutes. The bronchoconstriction reflex was defined as the development of a slow labored breathing with exaggerated abdominal movements. The onset of bronchoconstriction correlated in time with greatly altered breathing patterns, recorded on a Grass polygraph, and a pronounced wheeze. The two observers reported the onset occurred after 199±59 seconds and 199±57 seconds respectively. Figure 2-4 denotes the dose-dependent response curves of citric acid in guinea pigs.

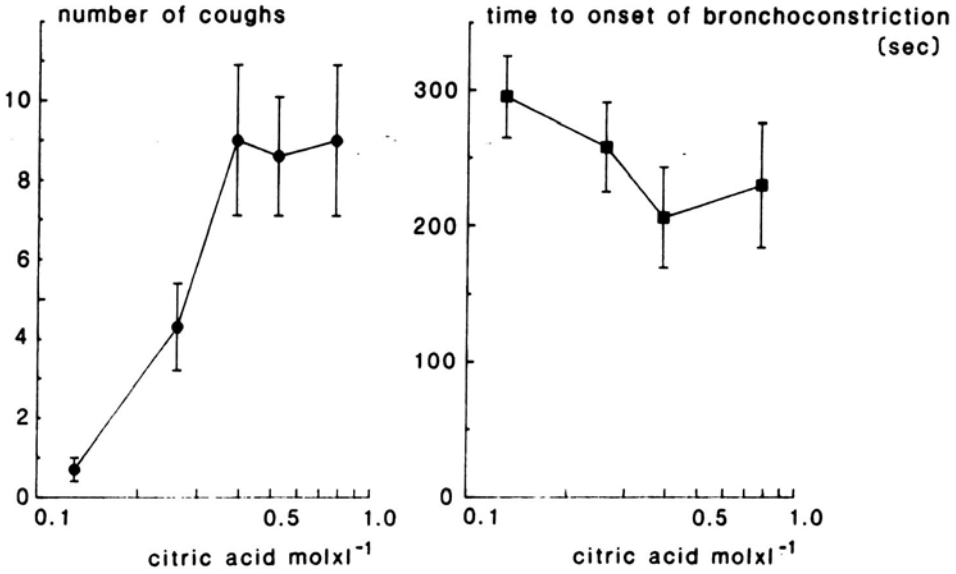

Figure 2-4 Guinea Pig Cough and Bronchoconstriction Dose Dependent Plots [24]

In this study, the onset of bronchoconstriction appeared to be independent of the cough response. It was noted that during some cough challenges, coughs

occurred before bronchoconstriction and in others bronchoconstriction occurred prior to coughs [24]. Based on these findings, the afferent pathways triggering broncho-constriction seem to be different than those that trigger cough [25]. These results, and other similar studies, have shown that citric acid induces cough and increases overall lung resistance in anaesthetized guinea pigs [26,27].

To summarize, citric acid had similar effects in humans and guinea pigs. Its provoked response seems to involve many of the same receptors and produce a similar cough response. Citric acid has been shown to cause bronchoconstriction and that the onset is unrelated to the cough response. This characteristic makes it possible to monitor the specific airway resistance created by reflex bronchoconstriction and to compare changes in the acoustical and flow characteristics at different stages of bronchoconstriction. Measuring the constrictive effects of citric acid on the airways while recording cough sounds will give insight into how the airway alterations change cough characteristics in guinea pigs. Findings in this data may indicate that coughs occurring after exposures to various occupational irritants can be measured and characterized in a similar fashion.

Chapter 3 – Materials and Methods

The development of an animal model for studying cough sound and flow measurements must meet several essential requirements. First and foremost, an appropriate animal must be chosen for the cough challenges. In addition, an exposure system must be developed to generate cough-inducing aerosols in a controllable fashion. Following an exposure, the system must also be capable of simultaneously recording cough sound and cough airflow measurements. Breathing pattern measurements must also be saved to calculate specific airway resistance at the time of the cough. It is essential that all data be saved so that synchronized measurements can be obtained during an experiment.

3.1 Animal Considerations

Based on previous studies, guinea pigs appear to be a suitable choice for an animal model. They are known to cough in response to irritants such as citric acid and capsaicin. They provide more consistent and reproducible coughs than rats and mice, and they have the advantage that they been used in many respiratory studies to approximate human respiratory system responses. Furthermore, they exhibit a cough response similar to that of humans.

The following protocol was used prior to exposing animals to conduct a cough challenge. Male Hartley guinea pigs were allowed to acclimate to their new environment for one week. After acclimation, they were loaded into the dual chamber plythesmograph used during the exposures for a minimum of three consecutive days to further acclimate them to the test environment. Once the smallest

guinea pig reached 300 grams, exposures began. This would allow approximately 10-12 days for testing before the animal grew too large for the plythesmograph.

3.2 System Hardware

The animal cough system is a multifunction apparatus. It is used both to expose the guinea pig to citric acid aerosols and record all cough sound and flow measurements after the exposure. A diagram of the complete system is shown in Figure 3-1.

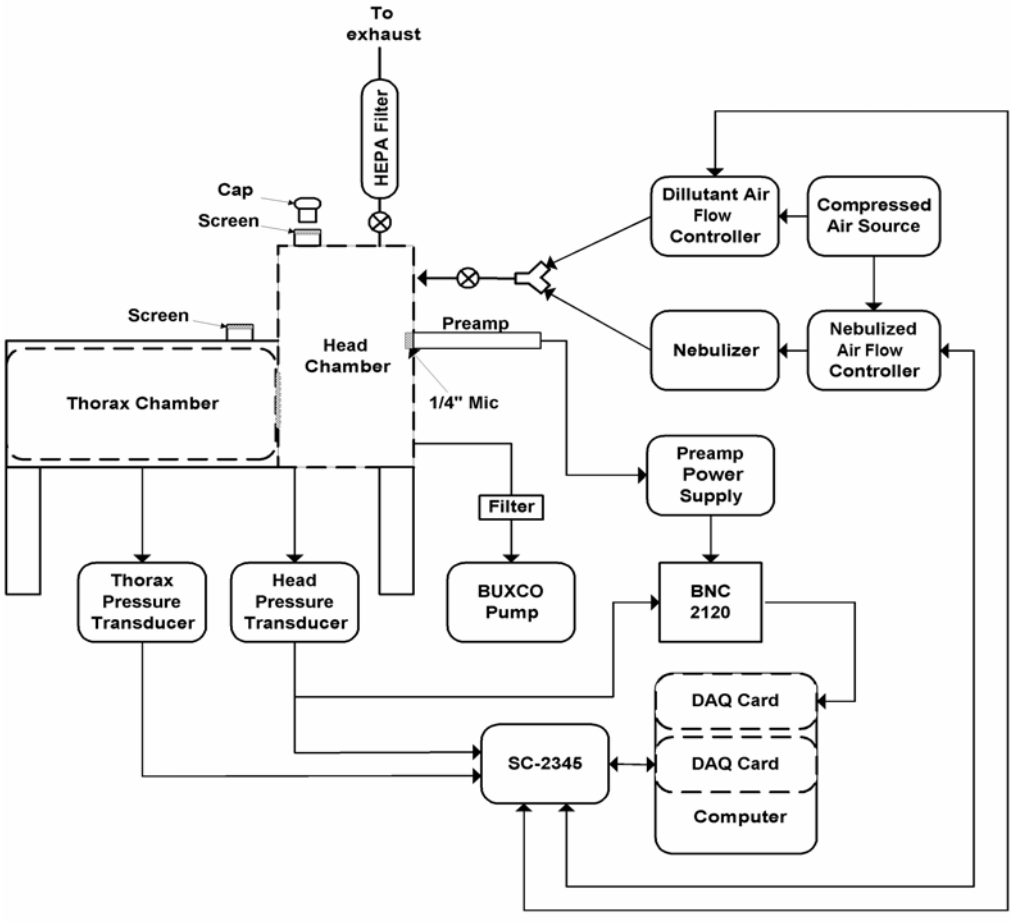

Figure 3-1 Block Diagram of Exposure and Cough Recording System

3.2.1 Citric Acid Exposure Components

Citric acid aerosols were created using a Devilbiss Ultra-Neb 99 nebulizer. In order to estimate the size and amount of aerosols present during the exposure, preliminary aerosol diameter and concentration measurements were obtained using a TSI model 3320 Aerodynamic Particle Sizer (APS) in the configuration shown in Figure 3-2. The APS measurements are taken from the aerosols present within the collection flask. The flask had a similar volume to that of the head chamber and was used to simulate the space present within the head chamber.

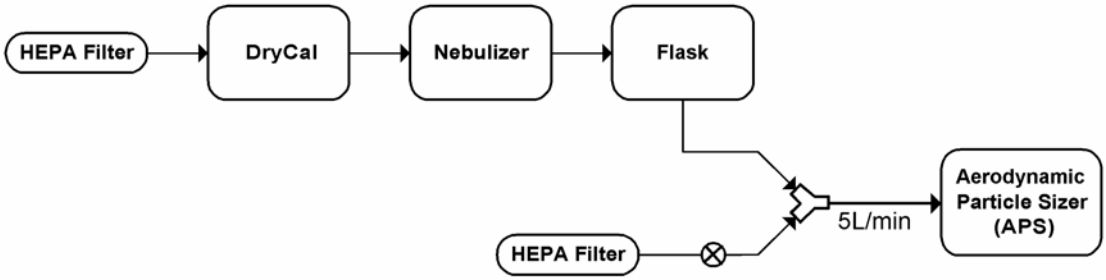

Figure 3-2 Diagram of System Used to Measure Nebulizer Aerosol Size Distribution

The APS draws a constant flow of 5L/min through the system. A flow calibrator (BIOS DryCal DC-Lite) was connected inline between the HEPA filter and nebulizer to accurately measure the nebulized airflow. By adjusting the valve between the intersection of the nebulized airflow and dilutant airflow and the lower HEPA filter, the nebulized airflow could be altered. Figure 3-3 is a plot of the measurements taken in a 30 second test period with a nebulized airflow of 0.35L/min. Based on the obtained data, 67% of the citric acid aerosols were less than 2.5um and 95% of the aerosols are less than 10um in size.

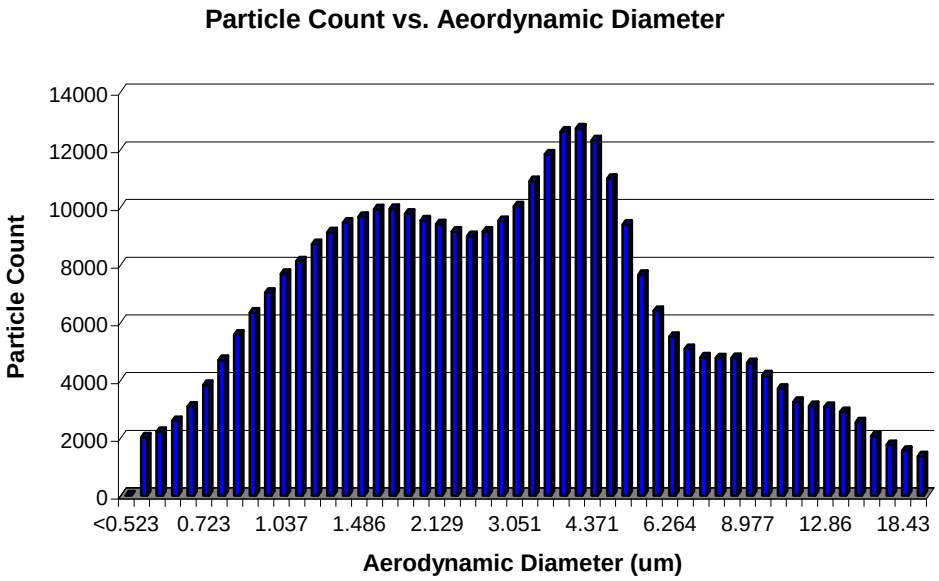

Figure 3-3 Aerosol Generation for the Devilbiss Ultra-Neb 99 Nebulizer

When animals were exposed, the aerosols were delivered to the head chamber by flowing air through the nebulizer cup using a 0-5L/min Aalborg mass flow controller**.** A controllable dilutant air source was provided by a 0-10L/min Aalborg mass flow controller. Using both mass flow controllers, the aerosol concentration within the chamber can be increased or decreased rapidly at any time by remotely adjusting the flow rates using the developed software. Each mass flow controller is equipped with a 0-5V analog output indicating the flow rate and a 0-5V analog input used to set the desired flow rate. Flow rates are determined based on a linear relationship between voltage and flow. Hence, a 0V input results in no flow and 5V input corresponds to the maximum flow rate for the particular flow controller. Complete specifications for the mass flow controllers can be found in Appendix A. Lastly, to insure proper oxygen exchange during all testing procedures, a 0-2.5L/min Buxco bias flow vacuum pump was connected to the head chamber using 1/16" inner diameter tygon tubing to pull air into the chamber at a constant rate of 1.2L/min.

3.2.2 Cough Flow and Sound Measurement Devices

The dual chamber plythesmograph (Hugo Sachs Elektronik-Harvard apparatus) was equipped with screen type pneumotachs in both the head and thorax chambers. See Figure 3-4. The resistances of the screens remain constant so that airflow is directly proportional to chamber pressure, making it possible to measure airflow into and out of each chamber. An in-depth description of how the flow measurement was obtained from the pressure changes can be found in section 3.3.2**.** To measure the pressure changes, Setra model 239 differential pressure transducers are connected to each chamber. The pressure range for each transducer was -0.25 to +0.25 inches of water. The output voltage ranges from –2.5 to +2.5V and follows a linear relationship to pressure. See Appendix A for detailed specifications of the pressure transducers.

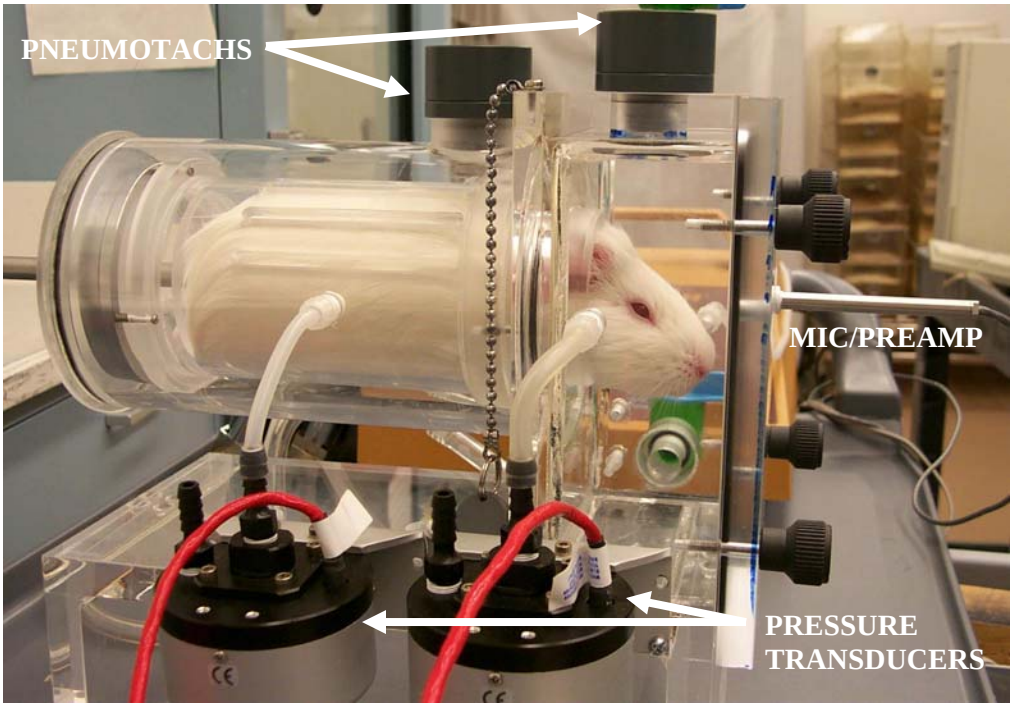

Figure 3-4 Digital Photograph of Dual Chamber Plythesmograph

Sound pressure waves were recorded using a Larson Davis audio setup consisting of: a model 2530 pressure and random incidence ¼" microphone, PRM910B ¼" preamplifier, and a 2200C dual channel microphone preamp/power supply. The microphone was located in the head chamber approximately ½" from the mouth of the guinea pig during the experiment. See Figure 3-4. The frequency response of the microphone was 4Hz - 80kHz, making it ideal for recording high frequency data. The microphone was matched with the preamp that was optimized for use with the precision condenser microphone. The microphone was powered by a 2200C dual channel preamp/power supply which offers attenuation and gain settings from –40 to +40dB relative to the input signal. The preamp/power supply furnishes a microphone polarization voltage setting of 28Vdc to properly match the microphone and conditions where it will be used. Outputs as high as 10Vrms are attainable for frequencies up to 50kHz, and the unit holds a long-term constant calibration level for changes in temperature and humidity. Refer to Appendix A for complete specifications of the audio equipment.

3.2.3 Data Acquisition System Overview

All devices were controlled by one of two Data Acquisition (DAQ) cards. A schematic of the complete DAQ system is shown in Figure 3-5. The National instruments (NI) 6036E DAQ card is a low cost multifunction DAQ card. The card features 2 analog outputs, 16 analog inputs with 16-bit resolution, and a peak sampling rate of 200 kS/s. Complete channel access is made possible via the NI SC-2345 signal conditioning box. The NI PCI-4451 DAQ card was selected for all audio acquisition. The card features 2 16-bit simultaneously sampled analog inputs with

sampling rates from 5 to 204.8kS/s, and 2 analog outputs. The appealing feature about this particular card is that all analog inputs have hardware implemented analog and digital filters. Input signals pass through the fixed analog filters to remove frequencies greater than the analog to digital converter's range. The digitized signal then passes through digital antialiasing filters that automatically adjust their cutoff frequency to remove frequency components above half the sampling rate. Complete specifications for these cards are located in Appendix A.

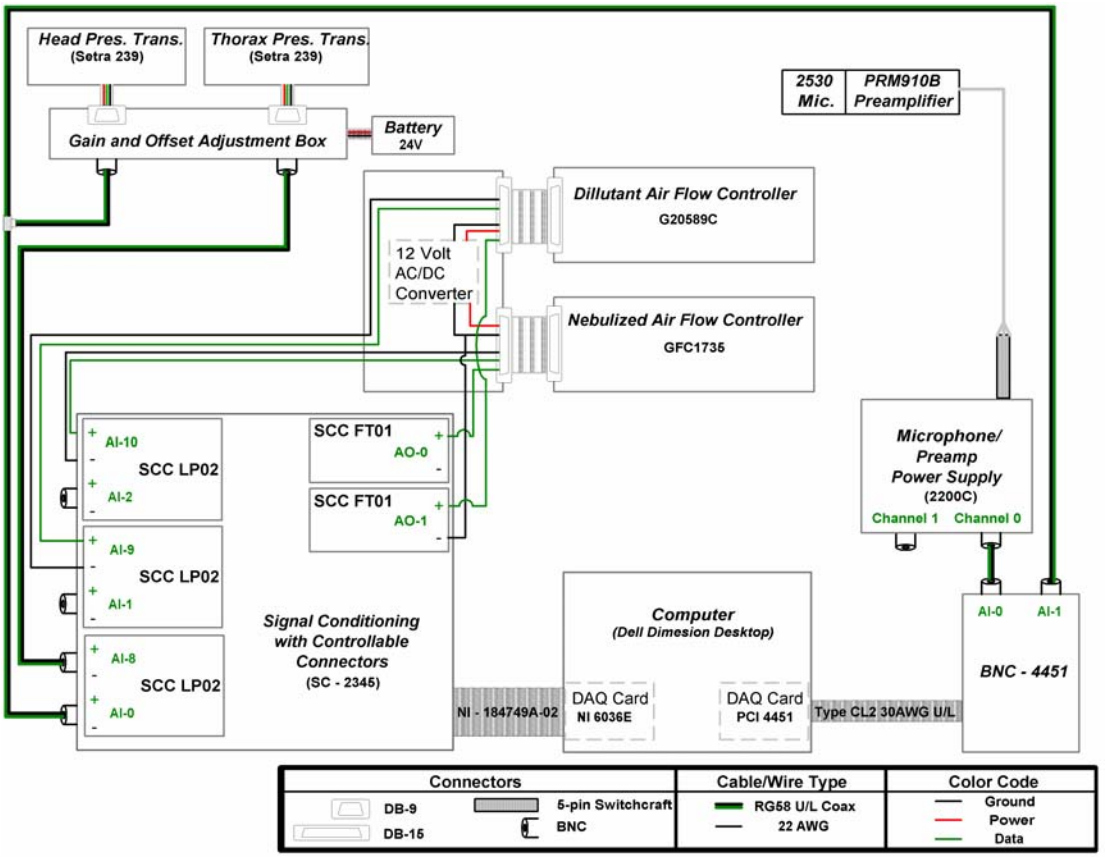

Figure 3-5 Electrical System Schematic

The NI 6036E DAQ is responsible for all data transfer to and from the pressure transducers and air flow controllers. See Figure 3-5. Pressure transducer analog outputs are first sent through a gain and offset adjustment box using a DB-9 connector. The gain and offset adjustment box is used to negate any DC offsets

found in the pressure signals. The box is also connected to a 24V battery to provide the required excitation voltage for the pressure transducers. The airflow controllers are connected to a junction box that powers both controllers and separates the analog input and analog output signals. The DC zeroed pressure transducer signals and the measured mass airflow readings are passed through a 4^{th} order 50Hz low pass Butterworth filter (SCC LP02) located within the signal condition box. The filter eliminates any noise readings greater than 50Hz from the signals and prevents frequencies greater than the cutoff frequency from being aliased as lower frequencies. The air flow controller analog inputs, used to set desired flow rates, are connected to analog output channels 0 and 1 of the NI 6036E DAQ card using the feed through connectors (SCC FT01) located inside the signal conditioning unit.

All sound measurements are recorded using the high fidelity NI PCI-4451 DAQ card. This DAQ card is mated to the BNC 4451 for access to the 2 analog inputs and 2 analog outputs provided on the card. The microphone/preamplifier combination is connected to the 2200C power supply using a 5-pin Switchcraft connector. The 2200C preamp/power supply amplifies the recorded sound pressure voltage from the microphone by 40dB before outputting the signal. As can be seen in Figure 3-5, channel 1 analog input is tied to the head chamber pressure signal. Since analog inputs are read simultaneously, this allows synchronized cough sound and flow measurements to be taken. Head chamber pressure signals recorded on channel 1 of the PCI-4451 DAQ card can then be correlated to the input from channel 0 of the NI 6036E DAQ card. Thorax pressure recorded using channel 8 of the NI 6036E DAQ card can be referenced to the recorded head chamber pressures recorded on

channel 0, enabling accurate synchronization of all flow and sound data. Complete specifications for both DAQ cards are located in Appendix A.

3.3 Development of LabVIEW Data Acquisition Code

National Instrument's LabVIEW 6i was the chosen software platform to meet the data acquisition requirements for the above system. LabVIEW is a visual programming language used to create virtual instruments (VIs) capable of controlling, monitoring, and saving all inputs and outputs of the system. It is compatible with both DAQ cards and has a broad range of configurable options. The following sections will discuss the LabVIEW VIs developed for calibration and data management.

3.3.1 Pressure to Flow Calibration Software

As described previously, pressure transducers are connected to the head and thorax chambers of the plythesmograph. In order to derive flow measurements based on pressure signals, a calibration constant was calculated for each chamber and used for the remainder of the experimental testing. Figure 3-6 is a screenshot of the calibration front panel. Among the "SETUP" options are: input volume, trigger level, number of scans to acquire, scan rate, pretrigger scans, and time limit. The input volume is the known air volume that will be injected into the chamber for calibration. Scan rate and time limit (timeout) can be adjusted based on user preference, and the number of scans are the total number of scans to acquire including the pretrigger scans.

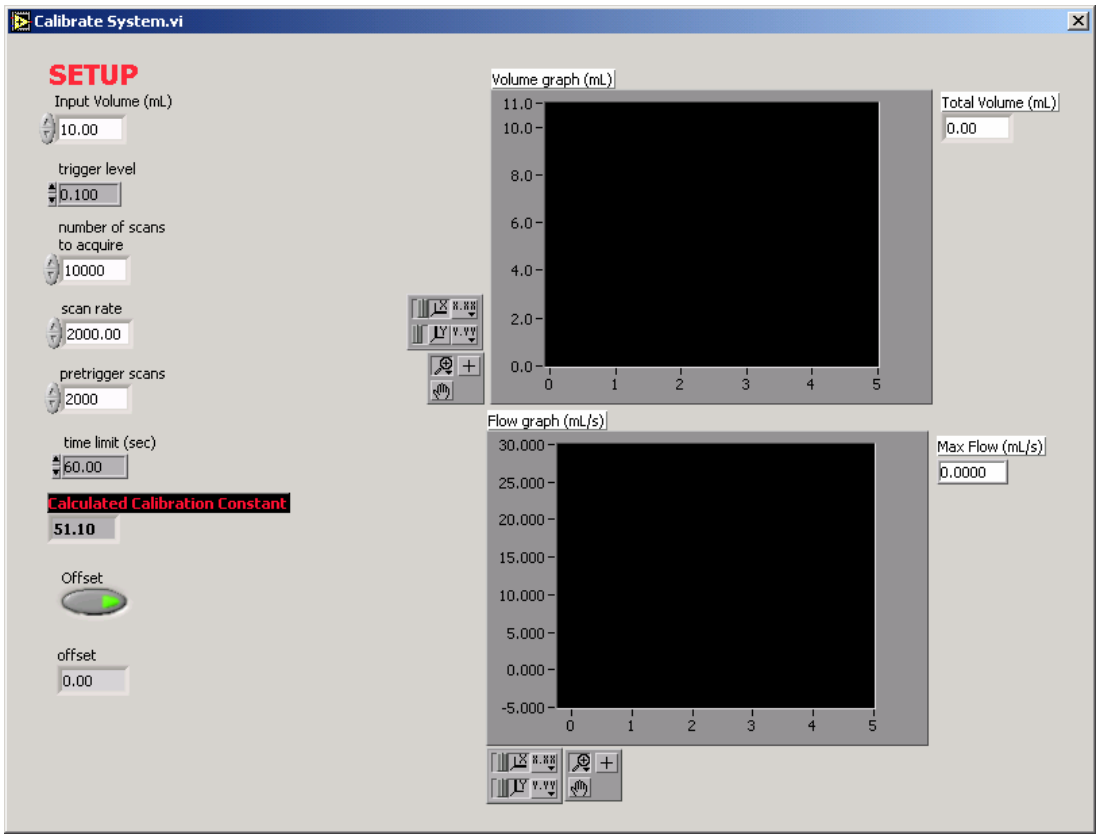

Figure 3-6 Calibration Software Virtual Instrument

In the present configuration, an air volume of 10mL is injected into the chamber using a 10mL syringe. The airflow created from the air being added to the chamber causes the voltage in the corresponding pressure transducer to increase. When the pressure transducer output voltage exceeds 0.1V, the implemented software trigger retrieves one second of previous buffered data and an additional four seconds after the trigger, insuring the entire pressure signal is captured. The captured data is sent to the conditional box (labeled as True) located in the center of Figure 3-7. Twenty pretrigger samples are averaged to calculate the DC offset in the signal. The offset is then subtracted from the original signal before any further calculations are made.

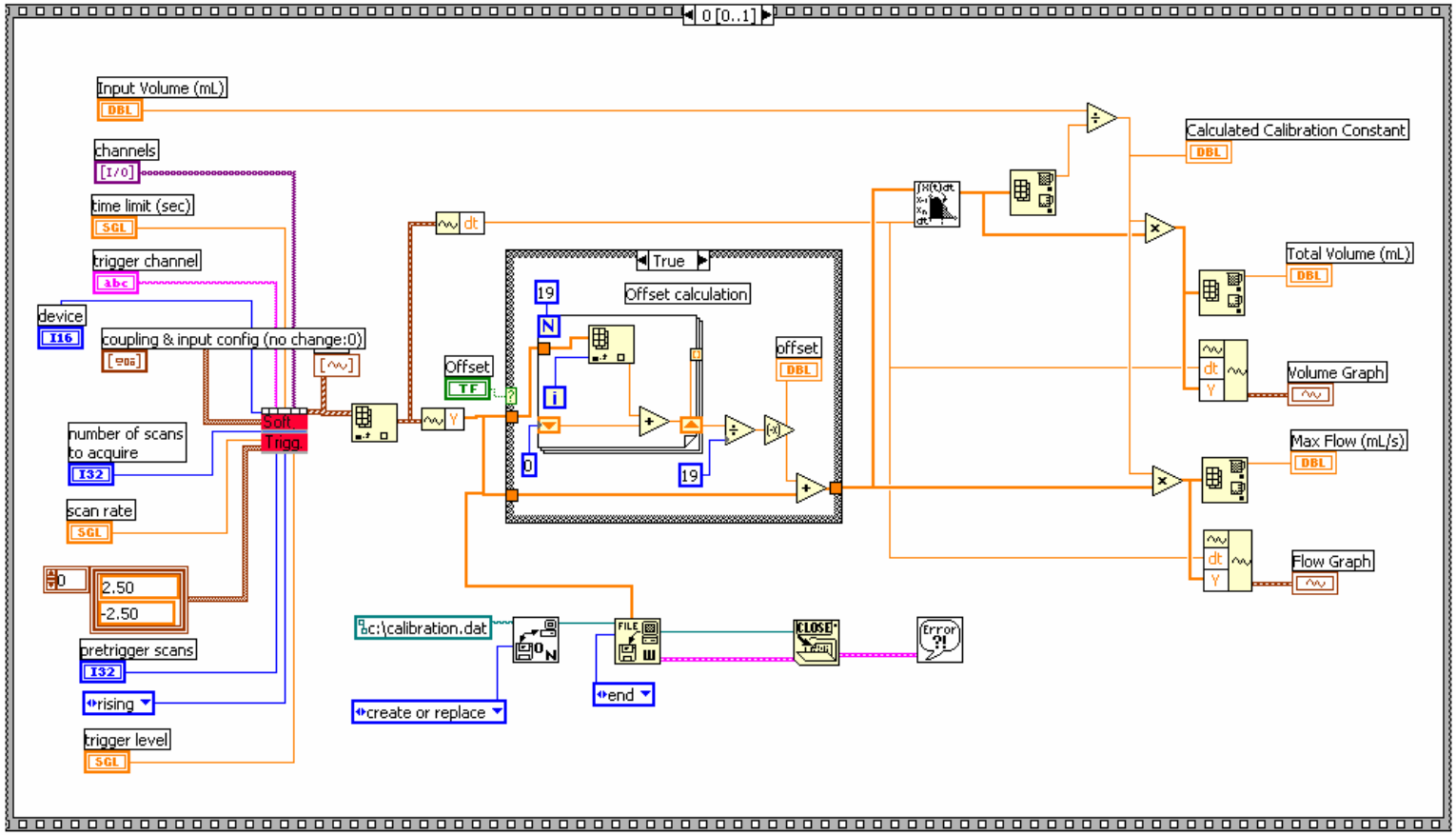

Figure 3-7 LabVIEW Code for Calibration Routine

The calibration constant and flow rate can be solved using Ohm's law by modeling the pressure, flow, and resistance of the calibration screens as a simple resistor circuit. Relating Ohm's Law to Pressure:

$$\Delta V = IR$$
$$\Delta P = (Flow)(R_{screen}) \quad (1)$$

$$Flow = \frac{\Delta P}{R_{screen}} \quad (2)$$

$$\int Flow = \int \frac{\Delta P}{R_{scren}} \quad (3)$$

$$\int Flow = Volume \quad (4)$$

$$Volume = \frac{\int \Delta P}{R_{screen}} \quad (5)$$

$$R_{screen} = \frac{\int \Delta P}{Volume} \quad (6)$$

$$1/CC = R_{screen} \quad (7)$$

where CC is the calibration constant

Therefore,

$$CC = \frac{Volume}{\int \Delta P} \quad (8)$$

As can be seen in upper right portion of Figure 3-7, equation 8 is used to calculate the calibration constant. In a series of three tests, *CC* was 50±3 in each chamber. The input volume is divided by the integrated pressure signal (the output from the conditional statement). The flow curve is calculated by taking the product of the pressure change and the derived calibration constant. The volume curve is calculated by integrating the pressure signal and multiplying it by the calibration constant. The resulting flow and volume curves after the calibration test are shown in Figure 3-8.

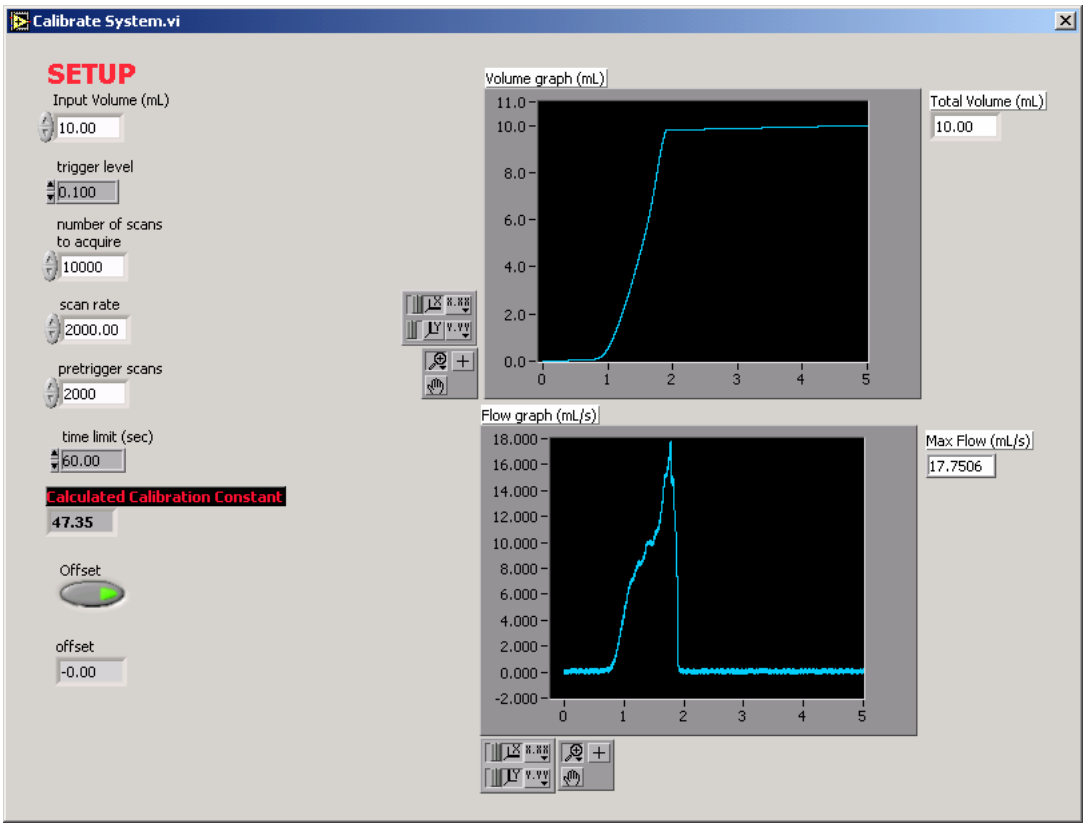

Figure 3-8 Calibration System Output

3.3.2 Front Panel Design and Operator Interface Description

The "Gpig Cough and Flow" VI, shown in Figure 3-9, is the next software component in the data acquisition system. This VI was created to control and monitor the citric acid exposure devices and the store relevant breathing, cough sound, and cough flow data obtained during the testing procedure. Before starting the software, the initial desired dilutant and nebulized airflows are set to zero. The head and thorax calibration constants, calculated from the calibration VI described earlier, are entered into the appropriately labeled text boxes located under the filtered cough plot area. At any time once the VI is started, head and thorax calibration constants can be recalculated by pressing the corresponding buttons located on the far left.

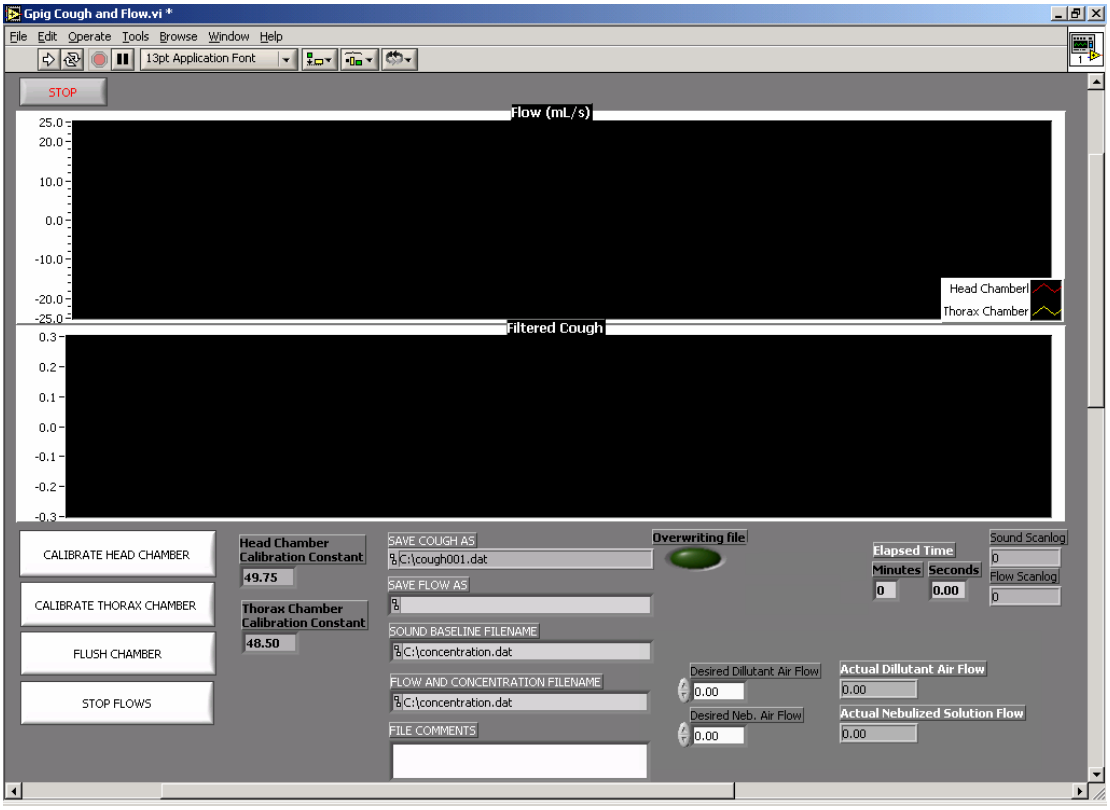

Figure 3-9 Exposure and Cough Acquisition Front Panel

After entering the needed inputs, the program can be started by pressing the small white arrow below the menu bar. As soon as the program starts, a dialog box is displayed requesting the user to input the date and guinea pig identification number used for the current exposure. See Figure 3-10.

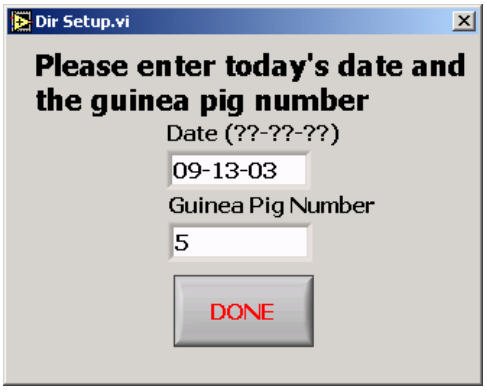

Figure 3-10 Directory Setup Dialog Box

Date and guinea pig information is used to create a directory structure and assign filenames for the data acquired during the exposure. Data content within each of the saved files is saved in a binary format to conserve disk space. Using the information entered in Figure 3-10, the following files would be created and opened for writing within the C:\09-13-03\gpig5\ directory.

- flowconc.fc5 – This file contains the raw voltage signals from both pressure transducers from the start of the exposure until the stop button is pressed. A header is written to the file containing the date, time, and length of the exposure. Also included in the header are the calibration constants, sampling rate (4000/S/s), and the text entered in the "FILE COMMENTS" in Figure 3-9.

- sound.base5 – This file contains a sample baseline sound file of the first 20 seconds of the exposure while the dilutant and nebulized airflows are turned off and the animal is in the chamber. In the post processing stage, this file will be used as a reference noise baseline. Header file includes date, time, sampling rate (98304S/s), and "FILE COMMENTS."

- cough###.dat – These files are 1 second sound files saved during the exposure when a potential cough occurred. (Cough detection will be explained in greater detail later in this section) The header of these files includes: date, time, sampling rate (98304S/s), elapsed time, and the acquisition backlog. File numbers begin at 1 and are incremented as potential coughs are recorded.

- flow###.dat – These are the corresponding flow files recorded from the head chamber. They contain the same header information as the sound files and are sampled at the same rate.

After the date and guinea pig information is entered and the user presses the "DONE" button, the designated filenames are displayed on the front panel. Pressure signals in the head and thorax chamber are converted to flow rates and updated to the front panel approximately every 0.15 seconds. See Figure 3-11. Dilutant and nebulized airflows can be changed at any time during the exposure by typing in the desired flow rates, or by using one of the two buttons located in the lower left position of the front panel labeled "FLUSH CHAMBER" and "STOP FLOWS."

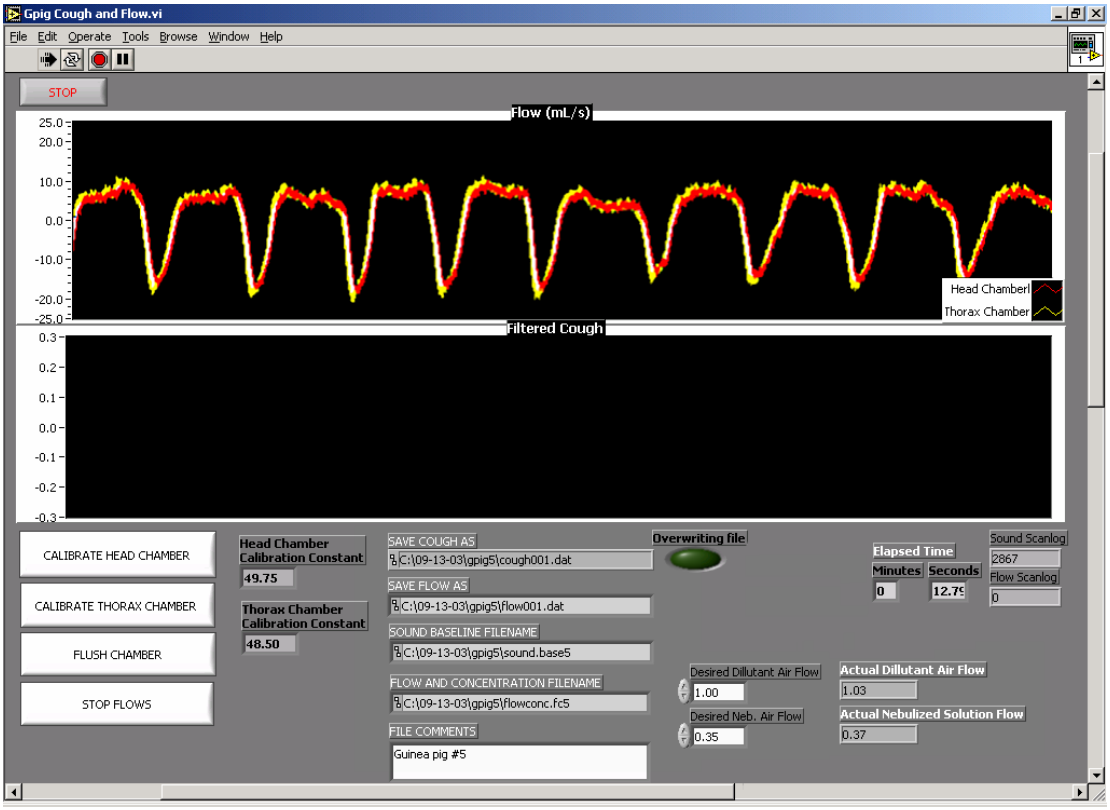

Figure 3-11 Exposure and Cough Acquisition Front Panel Displaying Measured Flow Rates

While the thorax and head flow rates are being displayed and recorded in the flowconc.fc# file, data from both channels of the PCI-4451 DAQ card are being sampled. As noted earlier, channel 0 corresponds to the microphone signal and channel 1 is the pressure in the head chamber. Each channel is read using a series of prepackaged LabVIEW analog functions. Analog input functions were configured to sample at 98304 S/s and store data into a 196608 sample (2 second) buffer. All data within the buffer is read and cleared by an analog read executed in the main loop of the program. The inputs from both channels (labeled as Sampled data in Figure 3-12) are parsed and recorded in separate circular buffers, each 1 second (98304 samples) in length.

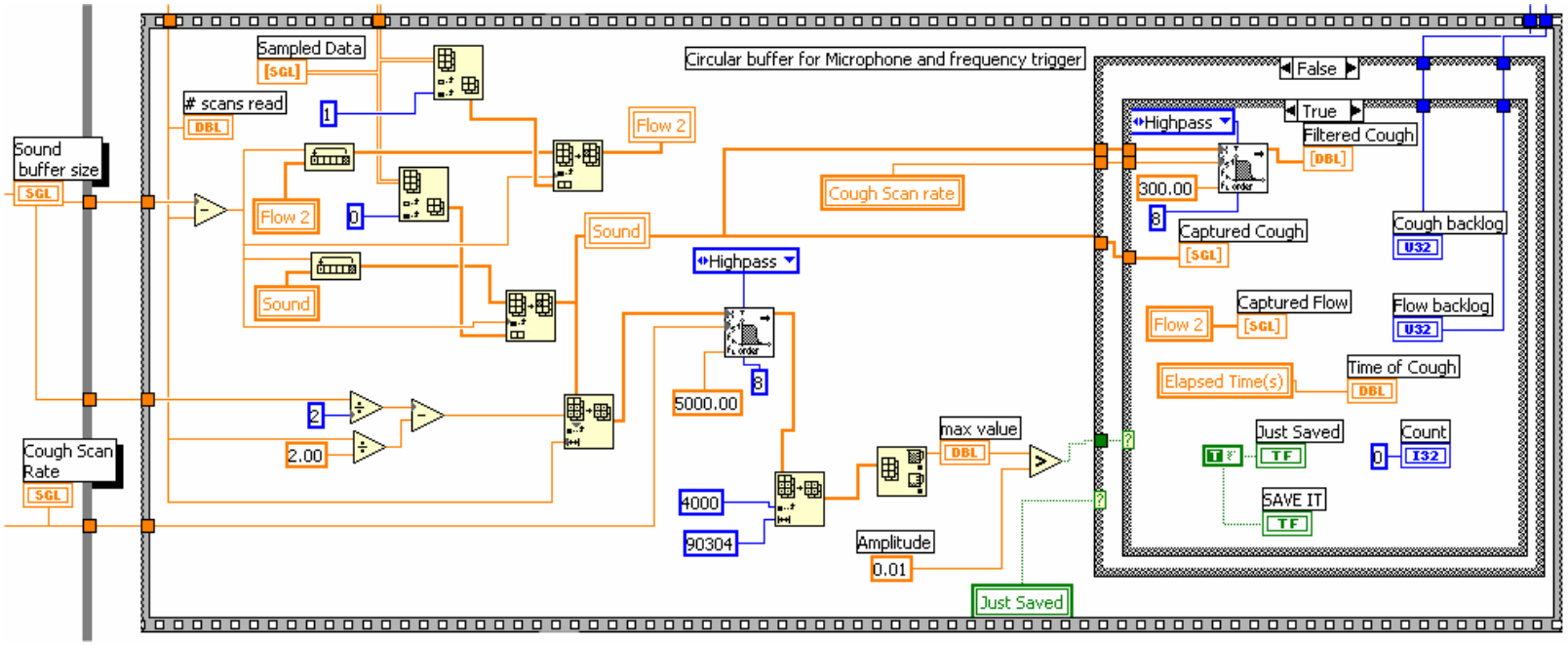

Figure 3-12 LabVIEW Code for Circular Buffers and Frequency Trigger

A specialized software trigger was created to examine the sound data to determine if a cough occurred. The trigger is designed to look at the samples located in the middle of the sound buffer and determine if frequencies above 5000Hz exceed an amplitude of 0.01V. In Figure 3-12, the position of the first sample of the data to be examined is obtained by dividing the buffer in half and subtracting half of the number of scans read each time through the loop. The last sample in the data is the position of the first sample plus the number of samples read during a single read process. This segment of buffer is sent to an 8^{th} order 5kHz high pass Butterworth filter. The max value of the output from the filter is compared to the desired amplitude. If the recorded sound exhibits frequency components greater than 5kHz and data was not stored from the buffer one read cycle earlier, the conditional statements on the far right are executed. Inside the conditional statements, the entire unfiltered sound buffer (labeled as Sound) and the corresponding flow buffer (labeled as Flow2) are saved. The unfiltered data in the cough buffer is then filtered using an 8^{th} order 300Hz high pass Butterworth filter and the resulting cough waveform is plotted in the front panel as shown in Figure 3-13. The cough and cough flow files are incremented and the system is ready to record the next cough.

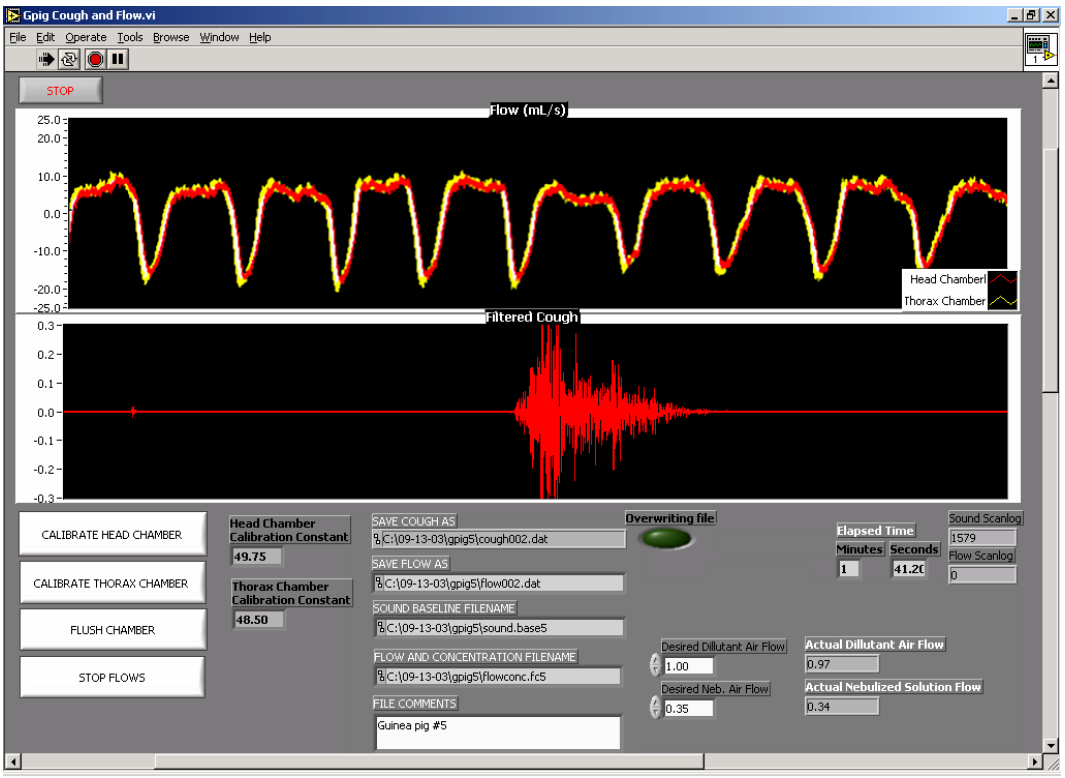

Figure 3-13 Exposure and Cough Acquisition Front Panel Displaying Triggered Cough

Once the cough challenge is complete, the user can press the stop button located at the top left corner of the front panel. The flowconc.fc5 file, containing pressure transducer outputs, is then closed. Before the next guinea pig is loaded into the chamber, the system can be flushed with dilutant air removing the majority of residual aerosols within the head chamber.

3.3.3 System Testing

One of the major concerns in the design of the acquisition software was the synchronization of the cough sound and flow data. In order to reliably relate flow and sound during the cough, it is important that the microphone and the head pressure transducer signals be synchronized. An experiment was designed to determine the accuracy of the designed software and the differences in response time for the

microphone and the head chamber pressure transducer. In order to do this, a small inflated balloon was placed in the head chamber and pricked. The sound and flow data were examined to ensure that the sound and flow measurements were in phase. In a series of three tests, the pressure transducer had an average delayed response of 108 samples resulting in a .0011 second slower response time.

3.4 Experimental Procedure

Two groups of six guinea pigs were used for the exposures. Nebulized airflows and exposure stopping criteria were determined based on preliminary cough challenges. See Table 3-1. The goal of the preliminary testing was to generate exposure guidelines for triggering coughs at different levels of bronchoconstriction. In order to minimize bronchoconstriction and consistently trigger the cough response, the nebulized airflows were set between 0.3 and 0.35L/m and the exposure was halted immediately after the first cough effort. By increasing the nebulizer airflow and delaying measurements until the second cough, the onset of bronchoconstriction was thought to occur earlier with an increased effect, thus producing coughs with increased airway resistance. As indicated in Table 3-1, three of the six guinea pigs in each group were exposed to ozone for three hours at a aerosol concentration of 2ppm before the third day of the scheduled citric acid exposures. Ozone has been shown to increase airway resistance up to three hours post exposure and to slightly decrease airway resistance thereafter [35]. The ozone exposure, in combination with varying nebulizer airflow settings and stopping criteria, enabled cough data to be collected with an increased variance in airway resistance.

Table 3-1 Guinea Pig Exposure Parameters and Stopping Criteria

Days from Initial Citric Acid Exposure	Elapsed Time since Ozone Exposure	Nebulized Airflow (L/min)	Exposure Stopping Criterion
0 (n = 12)	NE	0.3 - 0.35	First Cough Effort
1 (n = 12)	NE	0.35 - 0.4	Second Cough Effort or Evident Bronchoconstriction
2 (n = 6)	NE	0.3 - 0.35	First Cough Effort
2 (n = 6)	~ 15 min (c = 3 hours @ 2ppm)	0.3 - 0.35	First Cough Effort
3 (n = 6)	NE	0.3 - 0.35	First Cough Effort
3 (n = 6)	18 hours (c = 3 hours @ 2ppm)	0.3 - 0.35	First Cough Effort
7 (n = 6)	NE	0.35 - 0.4	Second Cough Effort or Evident Bronchoconstriction
7 (n = 6)	5 days (c = 3 hours @ 2ppm)	0.35 - 0.4	Second Cough Effort or Evident Bronchoconstriction

c = ozone exposure level

n = number of animals studied

NE = not exposed

Before conducting each exposure, all airflows were turned off and a calibration stopper was placed in the removable cylinder of the plythesmograph to provide an airtight seal between the head and thorax chamber. DC offsets from the pressure transducers were zeroed using the gain and adjustment offset box in conjunction with the test panel in the NI Measurement and Automation software package. Calibration coefficients for each chamber were determined and any air leaks in the system were remedied.

Upon successful calibration, a prepared 50mL solution of 0.39M citric acid was placed into the nebulizer cup, and all test animals were weighed. Guinea pigs

were then loaded individually into the removable slotted tube of the plythesmograph and positioned so that the flexible plastic seals fit snugly around the animal's neck. The removable tube and guinea pig were then placed horizontally into the plythesmograph. For the remainder of the experiment, a constant flow of 1 liter/min from the Buxco pump was provided to the head chamber. All valves remained closed, and only the holes with the screens were open. This is the configuration in which all acoustical and flow measurements were recorded.

Once the animal was relaxed inside the chamber, the data acquisition software was started. Initial breathing measurements were taken during the first 20 seconds in the current configuration. After the initial 20 seconds, the system was converted to begin delivering citric acid aerosols to the head chamber of the plythesmograph. The nebulizer was turned on, the exhaust valve and the nebulized/dilutant airflow valve were opened, and the cap was placed in the head chamber opening to prevent citric acid aerosols from leaking out of the head chamber. The nebulized airflow was set based on Table 3-1, and the dilutant airflow was held constant at 1L/min throughout the exposure. The citric acid exposure was stopped based on the criterion in Table 3-1. Once the stopping criterion was met, the plythesmograph was then reverted to the measurement phase described earlier with the cap removed from the head chamber and all valves closed. Cough sound and flow data was recorded for up to 10 minutes after the exposure. The guinea pig was then removed from the chamber and the head chamber was flushed with dilutant air at a rate of 10L/min for 30 seconds.

Chapter 4 – Data Processing Methods

After acquiring data using LabVIEW and associated hardware, post processing was performed in Matlab. Although LabVIEW is capable of real time data processing, all data stored during the data acquisition process was saved in its raw format for later analysis. The following chapter is an in-depth explanation of the data extraction process and the methods used to generate the cough parameter spreadsheet. The results from the data processing algorithms in this chapter will be presented in Chapter 5.

4.1 Specific Airway Resistance

There are many methods used to estimate airway resistance [39, 41]. Specific airway resistance (sR_{aw}), a commonly used noninvasive airway resistance estimation technique, uses dual chamber plythesmography [41]. In this analysis, sR_{aw} (airway resistance times thoracic gas volume) estimates airway resistance by assuming the thoracic gas volume of the lungs remains fairly consistent throughout the exposure. sR_{aw} provides a metric for quantifying the aerosol-induced bronchoconstriction present during each cough.

An efficient method was developed to estimate sR_{aw} near the time of the cough by analyzing the pressure changes across the screens in the head and thorax chamber during guinea pig respiration. Using the recorded pressure changes, the nasal and thorax flows can be calculated given the flow resistance of the screens in each chamber. The flows entering and exiting the chambers as a result of the drive in the thorax can be modeled as an electrical circuit (See Figure 4-1). Pressure (inches

of H_2O) is analogous to voltage, current represents the flow of gas in mL/s, and resistors are viewed as the resistance to flow in (inches of H_2O)/mL/s.

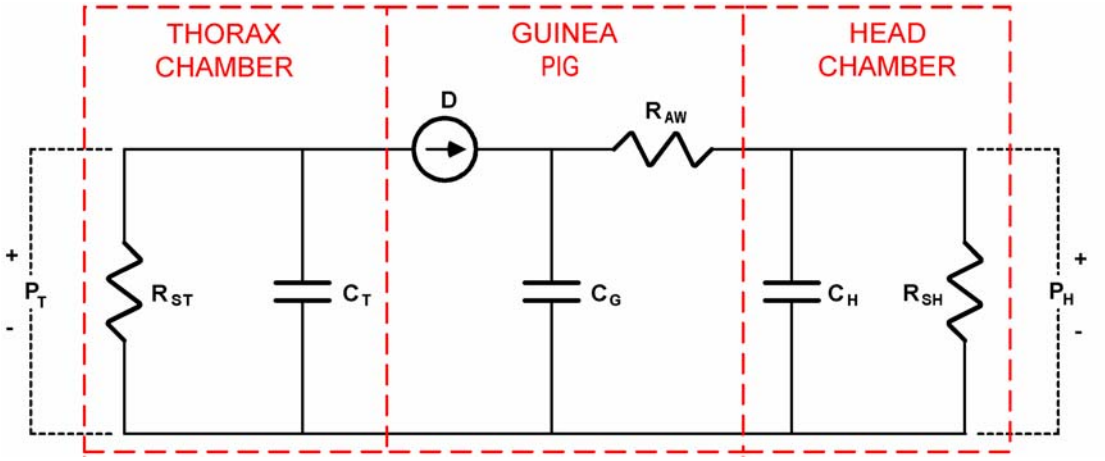

Figure 4-1 Electrical Flow Model of Guinea Pig in the Dual Chamber Plythesmograph

P_T and P_H are the thorax and head chamber pressure readings recorded in the flowconc.fc# file during the exposure. R_{ST} and R_{SH} are the resistance of the screens in each of the chambers, and C_T and C_H are the capacitance or compliance in ml/inchH_2O due to the volume present within the chambers. The current source D is the flow created by the driving force of the guinea pig's thorax. C_G is the capacitance of the thoracic gas volume present in the lungs, and R_{aw} is the resistance of the airways. By combining the resistance and capacitance in each chamber into a lumped impedance, the circuit can be rewritten where Z_T and Z_H represent the combined impedance of the screens and volume in each of the chambers. See Figure 4-2.

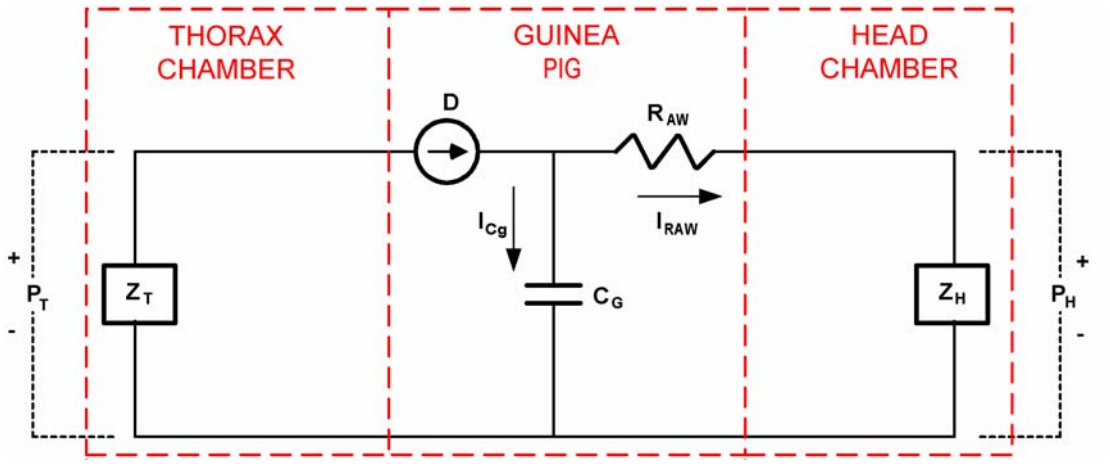

Figure 4-2 Simplified Electrical Flow Model of Guinea Pig in the Dual Chamber Plythesmograph

Using Kirchoff's Current Law, the currents in the circuit in Figure 4-2 can be expressed using the following equations.

$$D = i_{CG} + i_{RAW}$$

$$\frac{P_T}{Z_T} = C_G\left(\frac{R_{AW}}{Z_H} + 1\right)\frac{dP_H}{dt} + \frac{P_H}{Z_H}$$

Taking a Laplace transform of the above equation and expressing P_T as the input of the system and P_H as the output produces the following transfer function.

$$\frac{P_H}{P_T} = \frac{Z_H \big/ Z_T}{C_G\left(R_{AW} + Z_H\right)s + 1}$$

where

$$Z_T = \frac{R_{ST}}{R_{ST}C_T s + 1}$$

$$Z_H = \frac{R_{SH}}{R_{SH}C_H s + 1}$$

See Appendix B for a complete derivation of the circuit equation and transfer function.

The goal is to quantify how the change in specific airway resistance changes the spectral components of the cough sound. Since the actual airway resistance is not as critical to this analysis as is the change in airway resistance, the system transfer function can be simplified based on the following assumptions. The first assumption is that Z_T and Z_H are equal. The capacitance (change in volume/pressure) in each chamber is assumed to be nearly equal since the chambers have similar volumes and the pressure changes within the chamber are minimal. The resistance of the screens, R_{SH} and R_{ST}, as defined in Section 3.3.1 is the inverse of the calibration constant *CC*. *CC* was calculated to be 50±3 mL/s·Volt in both chambers. The pressure transducer voltage resolution is 0.1inchH_2O/V. Therefore, the resistance of the screens can be calculated as *R* in the following equation.

$$R = \frac{1}{CC} = \frac{1}{50mL/V \cdot s} = \frac{1}{50mL/0.1inchH_2O \cdot s} = .002\frac{inch \cdot H_2O}{mL/s}$$

By assuming both the capacitance of each chamber and the resistance in each chamber are equivalent, then $Z_T \approx Z_H$.

The second assumption is that the impedance in the head chamber, Z_H is very small in comparison to the resistance of the airways. Comparing airway resistance measurements obtained by Pennock et al with the chamber airflow resistance calculated above supports this assumption. Pennock found guinea pig airway resistances at different stages of bronchoconstriction to range from 0.2 – 1.77 $\frac{inchH_2O}{mL/s}$ using a pleural catheter [41]. Since the resistance of the screen accounts for <1% of the total resistance, the impedance $(R_{AW} + Z_H)$ in the denominator of the

transfer function can be approximated as R_{AW}. Following these assumptions, the transfer function can now be expressed in terms of P_T, P_H, C_G, and R_{AW}.

$$\frac{P_H}{P_T} = \frac{1}{R_{AW}C_G s + 1}$$

Since P_T and P_H are synchronously recorded, $C_G R_{AW}$ was determined in Matlab using the least square fit algorithm by rewriting the transfer function in the time domain.

$$P_H(t) = R_{AW}C_G \cdot \frac{dP_T(t)}{dt} + P_T(t)$$

$R_{AW}C_G$ was calculated by finding the coefficient that produced the least squared error in the time domain expression of the transfer function. To evaluate the fit, the head chamber flow (P_H *x CC*), thorax chamber flow (P_T *x CC*), and simulated flow from the above equation was plotted as shown in Figure 4-3.

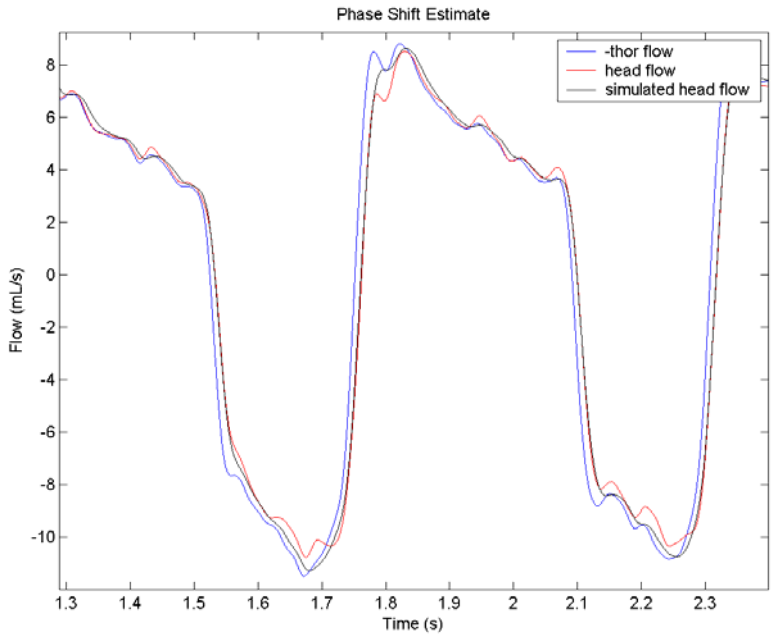

Figure 4-3 Head Chamber Flow, Thorax Chamber Flow, and Simulated Head Chamber Flow

Given that $R_{AW}C_G = R_{AW} \cdot TGV/P_B$ and $sR_{aw} = R_{AW} \cdot TGV$, sR_{aw} and can be calculated from $R_{AW}C_G$ by multiplying by the barometric pressure P_B. Since the change in $R_{AW}C_G$ is equivalent to the change in sR_{aw}, the correlation between cough characteristics and airway resistance were made using the time constant between the nasal and thorax breathing signal, $R_{AW}C_G$.

4.2 Acoustical Analysis

4.2.1 Data Extraction

Matlab software was developed to read in all potential coughs saved during the data acquisition process. Before developing cough statistics for each acquired potential cough, the saved data was played at $1/6^{th}$ the sampling rate to discriminate between coughs, sneezes, growls, or other noises (animal movement, squeals, etc) that may have inadvertently triggered the acquisition. Growls and noises were easily distinguished from coughs and sneezes by playing the cough sound at a reduced sampling rate. In most cases, coughs played at the reduced sampling rate sounded similar to human coughs and were distinguishable from sneezes. Potential coughs that could not be distinguished audibly were not included in the dataset. Ideally, coughs would be correlated with known characteristics of a guinea pig cough to classify the recorded data. However, there is no previous referenced work accurately characterizing the acoustical waveforms of the guinea pig cough.

Each cough was saved in an appropriate directory with all other coughs obtained during the exposure. The final step before analyzing the cough was to find the beginning and the end of the cough. Figure 4-4 contains a plot of a cough in its

raw format and a filtered version obtained from an 8th order high pass 500Hz butterworth filter.

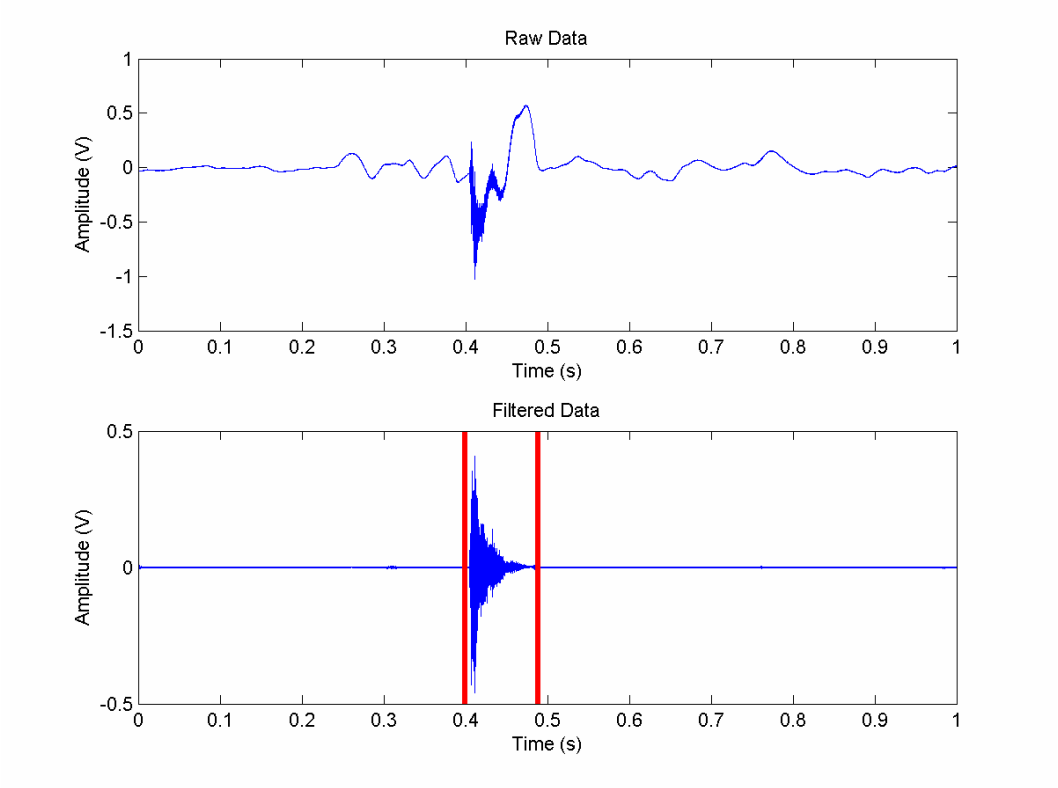

Figure 4-4 Time Domain Representation of Guinea Pig Cough

Cough start and end points were based on the amplitude of the filtered cough as indicated by the vertical red lines in the "Filtered Data" plot. The start and stop times of each cough were saved in appropriately named binary MAT-files and the cough length was recorded in the cough parameter spreadsheet. In the following cough sound and flow analysis, the cough files were loaded with the corresponding start and stop times, and only the data in the designated timeframe was analyzed.

4.2.2 Energy and Average Power

Since sound waves travel as waves of compression and rarefaction, sound measurements are typically calculated based on the sound pressure level (SPL). SPL is measured on a logarithmic scale in dB because sound pressures of various sounds tend to cover large ranges [40]. In this analysis, sound energy and power levels were calculated with standard signal processing equations by using the amplified voltage signal from the microphone instead of the actual sound pressure level. Energy was calculated from the time domain respresentation of the microphone voltage signal using the following equation.

$$Energy = \sum_{n=0}^{N} |x(n)|^2$$

The total energy of the signal was then divided by the sampling rate to convert energy to a time based energy measurement. Average power was calculated using the following equation [38].

$$Avg.Power = \frac{1}{N} \sum_{n=0}^{N} |x(n)|^2$$

where N = the number of samples
x(n) = time domain cough sound

By calculating energy and power based on standard signal processing equations, energy and power can be compared between coughs on a linear scale. The primary reason calculations were made this way was to provide proportionally weighted parameters since all other parameters were calculated on linear scales.

4.2.3 FFT

The fast Fourier Transform (FFT) is the mathematical basis of many of the spectral analysis techniques used to analyze cough sound data. The primary function of the FFT is to transform sampled data from the time domain to the frequency domain. The FFT works on the basis that the signal is composed of a number of sinusoidal components of various frequencies, amplitudes, and initial phases. The resulting sinusoids are then summed creating a frequency domain signal. To analyze discrete time signals, a variation of the FFT known as the discrete Fourier Transform (DFT) is used. The defining equation is as follows:

$$G(f) = \sum_{n=-\infty}^{\infty} g(t_n) e^{-j2\pi f t_n}$$

$G(f)$ is the frequency domain representation of the time domain signal $g(t_n)$ [36]. The DFT is the fundamental component in many of the data processing techniques in the following sections.

4.2.4 Power Spectrum

The power spectrum is used to calculate the power as a function of the frequency. Typically, a power spectrum analysis is more applicable to stationary signals. Coughs are better described as non-stationary signals since the frequency content changes throughout the cough. Although cough sounds are more characteristic of non-stationary signals, it was assumed that they can be divided into short quasi-stationary sections and analyzed as stationary signals [36]. In the analysis of the cough sound, Welch's method and Burg's method were used to analyze the

cough power spectrum. Welch's method is one of the more common methods used for analyzing the frequency power relationship. While examining the power spectra using Welch's method, the power in adjacent frequencies appeared to be quite oscillatory. Burg's method was used to provide a smoother power spectrum and capture the major characteristics. Cough parameters were derived using both power spectrums.

4.2.4.1 Welch's Method

The first step in Welch's method for estimating the power spectrum is to divide the time signal into successive blocks. The process of sectioning the time domain signal into smaller signals is called time windowing. Sliding the window across the time domain signal and calculating spectral intensity for that window in essence breaks the cough sound into stationary segments [36]. In the analysis of cough sound data, a 256 sample Hanning window was used with an overlap of 128 samples or half the window size.

Before calculating the power spectrum from each window, the individual windowed time domain signals were zero-padded by adding zeros to the time domain signal. Zero-padding is a technique that is often used to interpolate between frequency samples of a fixed length DFT and is effective in producing more frequency samples of the periodically replicated signal spectrum. Since a true improvement in spectral resolution can only be achieved using a longer time-duration window, zero padding is a somewhat artificial method for improving frequency resolution [38].

For each zero-padded time domain window, the spectral power using Welch's method was calculated by averaging the squared magnitude DFTs using the following equation:

$$Pxx(f) = \frac{1}{M}\sum_{m=0}^{M-1} |\, DFT_k(x_m)\,|^2$$

M denotes the number of windowed time samples and x_m is the time domain signal within the current segment. $Pxx(f)$ is the returned power spectrum estimate for the complete signal [38]. The power spectrum for a randomly selected cough using Welch's method with a DFT length of 2048 samples is shown in Figure 4-5. The frequency and magnitude corresponding to the highest peak in the cough spectrum were recorded in the cough parameter spreadsheet as the dominant frequency and peak power.

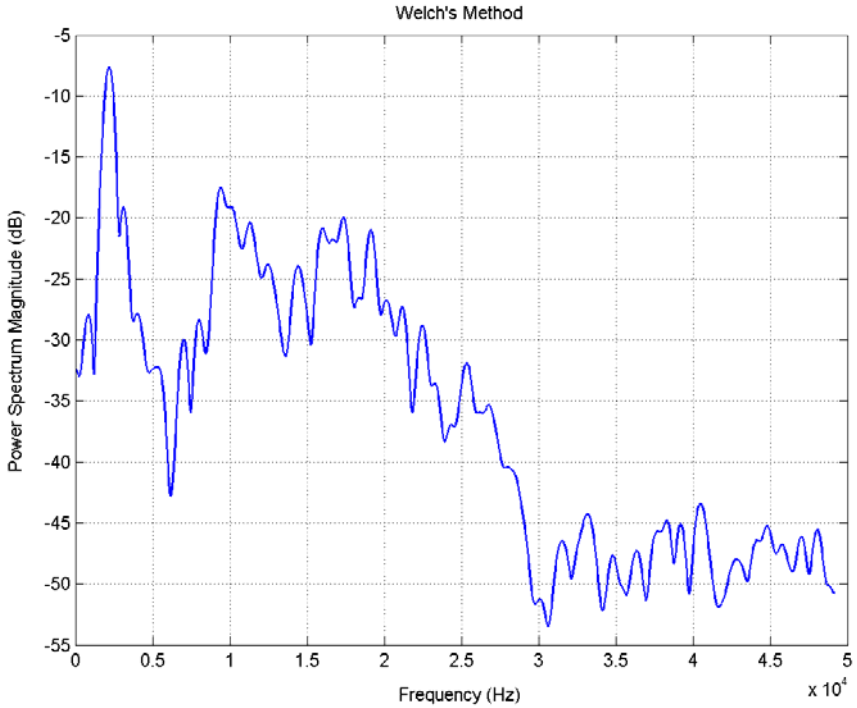

Figure 4-5 Welch's Power Spectrum

4.2.4.2 Burg's Method

The Burg method calculates the spectral density from the frequency response of an all-pole linear filter specified by the autoregressive (AR) linear prediction model. The first step in generating the power spectrum using this method is to calculate the coefficients of the following linear prediction model.

$$\hat{y}_p(t) = -\sum_{k=1}^{n} a_k y(t-k)$$

The current sample $y(t)$, is predicted from a linear combination of a finite number of past samples (n) yielding the predicted signal sample, $\hat{y}_p(t)$. n is the prediction order, and a is a vector of calculated model coefficients [19]. Using the least squares method, the Burg method calculates the best fit model of the input signal by minimizing the mean of the forward prediction error $f_n = y(t) - \hat{y}_p(t)$ and the backward prediction error $g_n = y(t-n) - \hat{y}_p(t-n)$ where

$$\hat{y}_p(t-n) = -\sum_{k=1}^{n} a_k y(t+k-n)$$

The resulting coefficients are constrained to satisfy the Levinson Durbin recursion algorithm [38]. From the derived coefficients, the input data is characterized using a source based all-pole transfer function, and can be written in the z-domain as

$$H_q(z) = \frac{\sqrt{e}}{1 + a_2 z^{-1} + a_3 z^{-2} .... + a_{(p+1)} z^{-p}}$$

where e is the variance estimate of the input to the AR model.

The complex frequency response is calculated by evaluating H_q at $z = (e^{j\omega})$ and performing a DFT on the numerator and denominator. The numerator is divided

point by point by the denominator yielding the complex frequency response vector of the prediction filter. The power spectrum is obtained from the product of the estimated AR model variance and the complex frequency response vector. The resulting power spectrum is shown in Figure 4-6 for the same cough as in Figure 4-5.

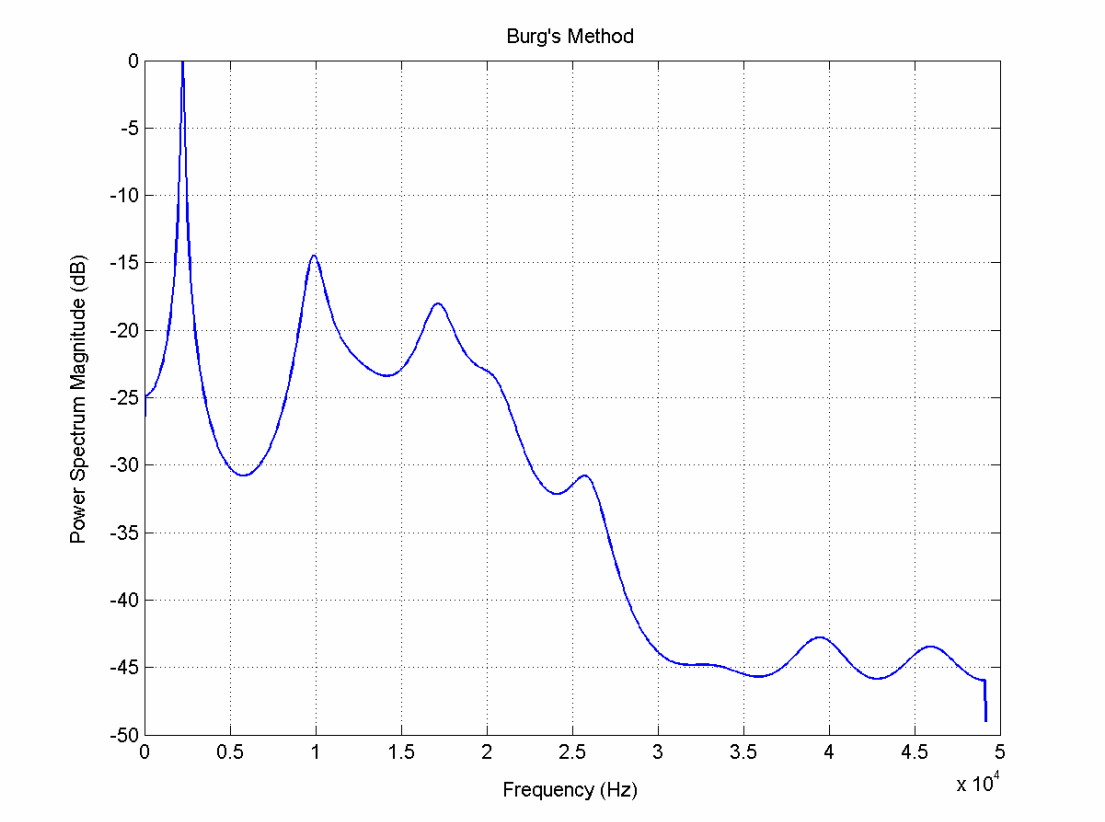

Figure 4-6 Burg's Power Spectrum

The prediction model order has an important role in the frequency response of the prediction filter, and is directly related to the number of poles in the filter transfer function. The peaks in the power spectrum of Figure 4-6 correspond to frequencies near the poles of the filter. In order to capture the main peaks of the power spectrum and eliminate the small oscillatory peaks seen using Welch's method, a 20^{th} order Burg model was selected. As can be seen in Figure 4-7, a 20^{th} order model produces a much smoother power spectrum while preserving the major characteristics.

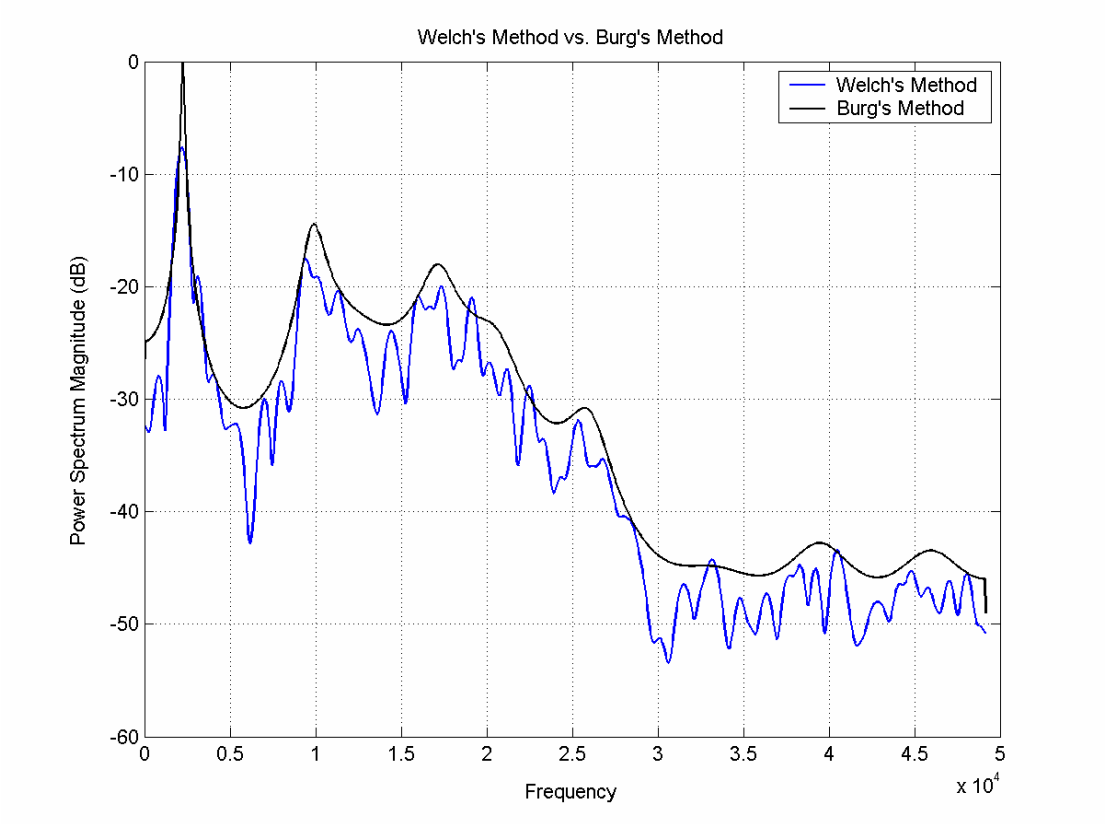

Figure 4-7 Comparison between Welch's Power Spectrum and Burg's Power Spectrum

In order to use the power spectrum as a parameter or group of parameters for correlating the cough sound spectrum with airway resistance, the peak power of the spectrum was recorded in conjunction with a set of estimated power spectrum parameters. Peak power was obtained from the maximum magnitude of the power spectrum, and the estimated power spectrum parameters were calculated by dividing the power spectrum into thirty-two 1500Hz non-overlapping frequency blocks and averaging the power in each block. The peak power and the estimated power spectrum parameters were saved in the cough parameter spreadsheet for later analysis.

4.2.4.3 Octave Analyzer

The power spectra of both Welch's method and Burg's method were split into seven octaves beginning at 500Hz. For a standard octave analyzer, the upper cutoff frequency in each octave is twice the lower cutoff frequency [37]. Figure 4-8 demonstrates how the power spectrum was split into different octaves using Welch's power spectrum.

Figure 4-8 Octave Breakdown Using Welch's Method

The percent power in each octave was calculated by dividing the power in each octave by the total power in the signal. The octave analysis was performed on the power spectra generated by both Welch's and Burg's power spectrum estimation methods. All octave percent powers for both spectrums were saved in the cough parameter spreadsheet.

4.2.5 Frequency vs. Time analysis

4.2.5.1 Spectrogram

A spectrogram is a time-dependent frequency analysis technique used to compare the cough spectrum with respect to time. The spectrogram splits the cough sound into overlapping sections specified by the window size and the number of samples each window is to overlap adjacent windows. For the cough sounds, a window size of 128 samples with a 96 sample overlap provided the best overall time (horizontal) and frequency (vertical) resolution. To calculate the short-term frequency content of the signal, each window was zero-padded to a length 2048 and the DFT was performed on each window. The color intensity in the spectrogram is representative of the frequency power during the cough. See Figure 4-9.

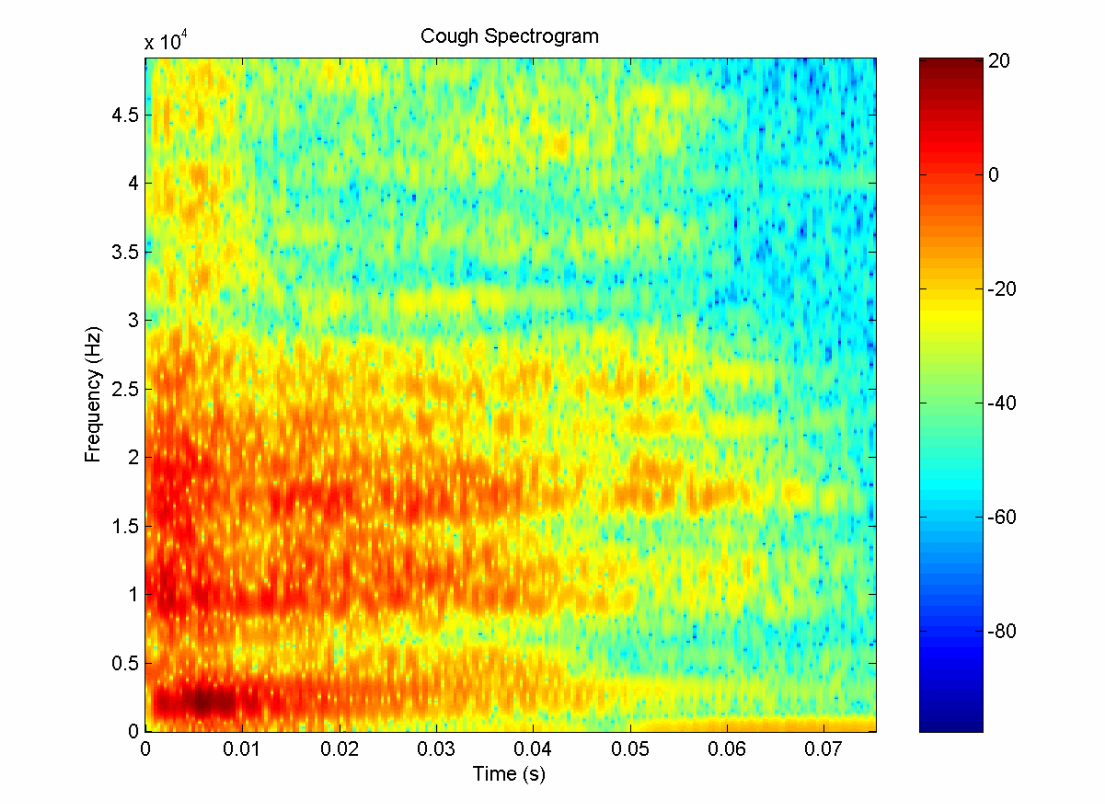

Figure 4-9 Guinea Pig Cough Spectrogram

4.2.5.2 Spectrogram Parameters

The Matlab specgram function outputs vectors *F* and *T,* and matrix *B*. Vectors *F* and *T* contain the range of frequencies and midpoint of the time window at which the DFT is computed. *B* is a (length of *F*) x (length of *T*) matrix composed of the frequency magnitude or power at *F* frequencies at *T* times.

To provide a quantitative feel of how the frequency or pitch changes during the cough, two methods were developed for characterizing the spectrogram. The first method calculates a weighted frequency average at different times during the cough. The output vector *T* is divided into thirty equally sized time frames. For each timeframe, *F* was multiplied by the corresponding frequency magnitudes found in *B*. The product of *F* and *B* was divided by the total frequency magnitudes in each respective timeframe; thus producing weighted average frequencies for all timeframes. The resulting vector is transposed on the spectrogram in Figure 4-10.

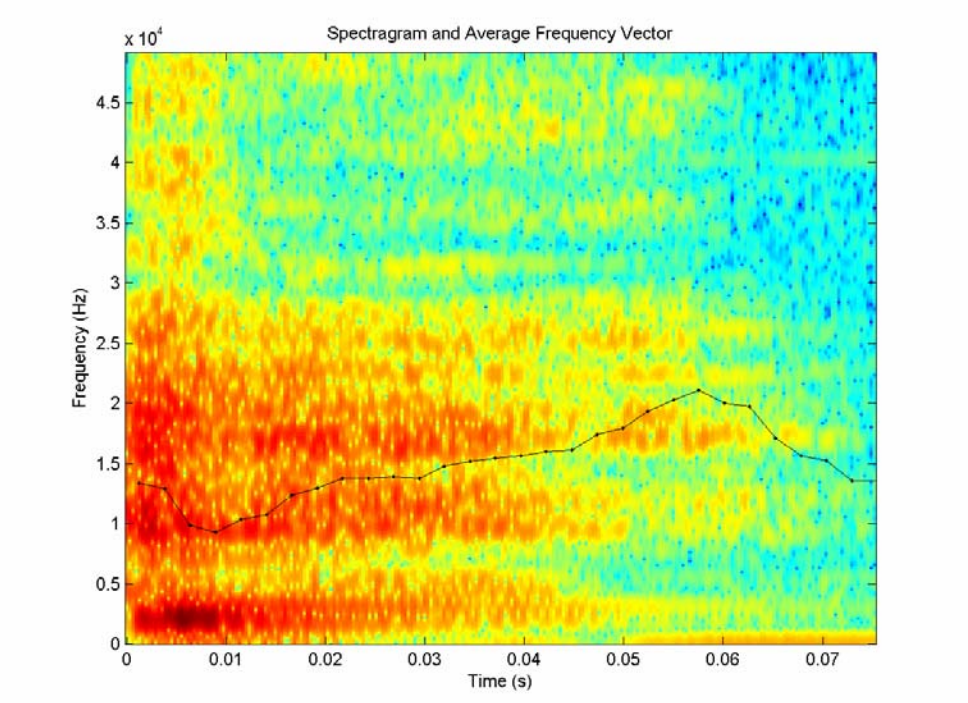

Figure 4-10 Average Frequency Vector

The next method is similar to the previously described method, except the weighted averaging is computed along the time axis. Instead of separating the cough into timeframes, the cough spectrum is broken down into 30 non-overlapping frequency bands. The product of the frequency power in each frequency band and *T* were divided by the respective frequency power obtained from matrix *B*. The resulting averages define the time at which the midpoint of the power occurs in each frequency band during the cough. See Figure 4-11. The horizontal lines are the frequency band divisions and the vertical lines are the power midpoint for each frequency band.

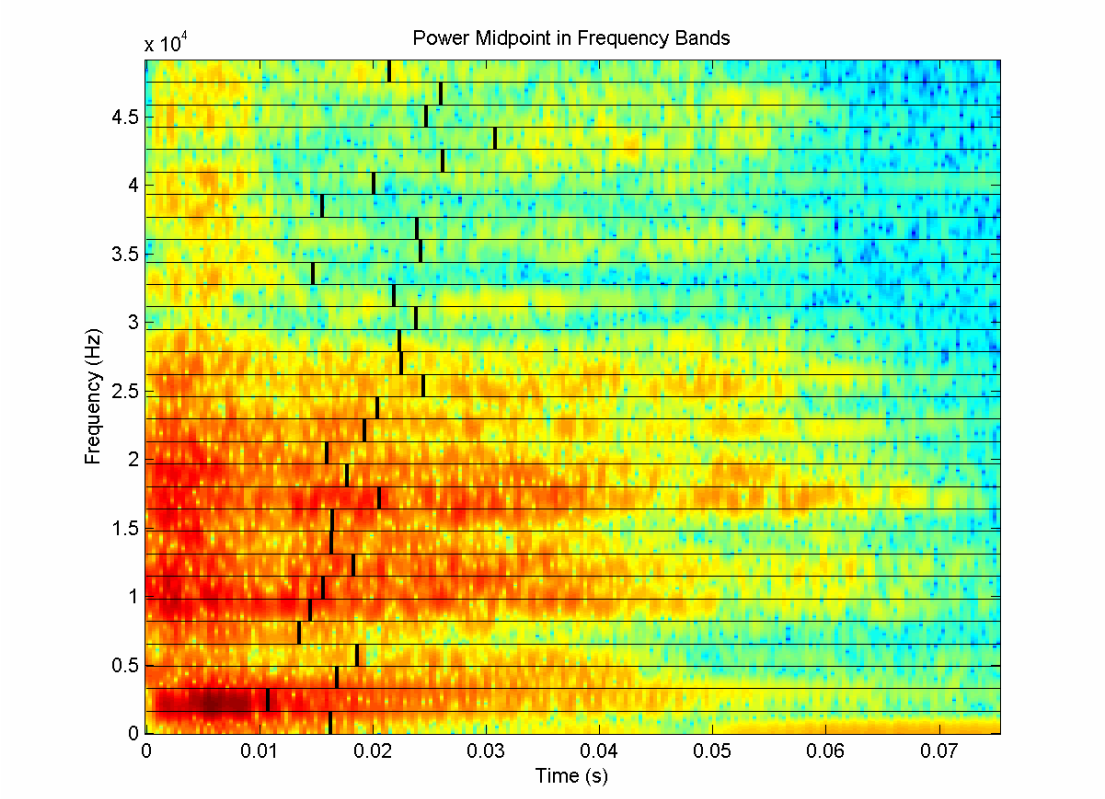

Figure 4-11 Power Midpoint in Frequency Bands

4.3 Cough Flow Analysis

Peak flow, average flow, peak acceleratory flow, and total expiratory volume parameters were calculated for all coughs. Flows were calculated by multiplying the head chamber pressure signal obtained during the cough by the calibration coefficient recorded in the header of each flow#.dat file. The maximum flow recorded during the cough was noted as the peak flow. The average flow was calculated by a point-by-point addition of all the flow values obtained during the cough divided by the total number of points in the cough length. Peak acceleratory flow (mL/s^2) was calculated by finding the peak value in the derivative of the flow signal. The total expiratory volume was calculated by integrating the flow signal for the duration of the cough.

4.4 Cough Characteristics vs. Airway resistance

Given the large number of cough parameters derived from the previously described methods, a fast, reliable approach was needed to quantify the relationship between the derived cough parameters and the time constant, $R_{AW}C_G$. The primary goal of the analysis is to determine how accurately coughs occurring at a low airway resistance can be distinguished from coughs occurring at a high airway resistance. The approach taken was a two-step process. The first step was to re-express the cough parameters through principal component analysis (PCA). The resulting cough parameters were then weighted and summed using a single neuron neural network thus providing a single output relating the cough sound to airway resistance.

Before processing the cough parameters, coughs were divided into three groups based on the average of the pre-cough and post-cough $R_{AW}C_G$ measurements. Groups 1, 2, and 3 were categorized of having low, moderate, and high airway

resistances respectively. Outliers within each group where determined by calculating the standard deviation of each parameter within the group. Coughs having 10% or more parameters exceeding two standard deviations from the mean of the group were considered poor coughs and removed from the dataset. This resulted in approximately 9% of the coughs being removed in each group. The resulting group statistics are in Table 4-1.

Table 4-1 Cough Group Statistics

Group #	RC range (s)	RC avg ± std (s)	# of coughs
1	0.0040 - 0.0060	0.0051±.00053	113
2	0.0060 - 0.0095	0.0073±0.0010	143
3	0.0095 - 0.0154	0.0117±0.0016	93

Group divisions were established to force the airway resistance measurements of group 3 to be approximately double that of group 1, while maintaining a considerable number of coughs in both groups. Group 2 contains the coughs in the transition from the low airway resistance coughs of group 1 to the high airway resistance coughs of group 3. The following chapter will primarily focus on the cough characteristics in groups 1 and 3 to discriminate coughs occurring at low and high airway resistances. To properly insure that the proposed analysis focuses on changes due to airway resistance and not the differences in cough characteristics of the guinea pigs in each group, the number of guinea pigs representing coughs in each group including the number of coughs exhibited by those guinea pigs were counted. Coughs in groups 1 and 3 were both comprised of coughs from ten guinea pigs. Eight of the ten guinea pigs exhibited a minimum of 73 coughs in both group 1 and group 3.

Each group was then subdivided to form train and test datasets. 75% of the coughs were used to construct the train dataset and the remaining 25% were used to form the test dataset. Coughs for each dataset were selected so that the specific airway resistance measurements for each dataset were statistically equivalent. See Table 4-2.

Table 4-2 Train and Test Dataset Statistics

Train Dataset			
Group #	**RC range (s)**	**RC avg ± std (s)**	**# of coughs**
1	0.0040 – 0.0060	0.0051±.00054	85
2	0.0060 – 0.0095	0.0073±0.0094	107
3	0.0095 - 0.0154	0.0117±0.0016	70
Test Dataset			
Group #	**RC range (s)**	**RC avg ± std (s)**	**# of coughs**
1	0.0040 – 0.0060	0.0051±.00052	28
2	0.0060 – 0.0095	0.0074±0.0010	36
3	0.0095 - 0.0152	0.0116±0.0017	23

The train dataset was used to calculate the principal component vectors and input weights for the neural net. Using the principal components and weights obtained from the train dataset, the test data was used to evaluate the accuracy of the developed analysis technique.

4.4.1 Principal Component Analysis

Principal component analysis (PCA) is a non-parametric mathematical method for extracting significant information from a complex dataset. The fundamental concept behind PCA is to define a new basis that best represents the variability in the initial dataset.

Consider X and Y to be m x n matrices related by a linear transformation P.

$$PX = Y$$

X is composed of m cough parameters for n guinea pig coughs. Y is the new representation of the initial dataset X, and the rows of P are the principal components that best express X.

P is defined in a way that minimizes the covariance between cough parameters and maximizes the variance within each parameter. This in essence eliminates the redundant information found between parameters and emphasizes the correlation within each parameter. To insure all parameter variances in X are considered equally, each cough parameter is divided by its respective mean. The mean of the resulting parameters in X are subtracted so each parameter has a mean of zero and an appropriately scaled variance. The variances and covariances of each parameter in X can be calculated with the following covariance matrix equation.

$$S_X = \frac{1}{n-1} XX^T$$

The diagonals of S_X contain the variance within each parameter, and the off-diagonal terms are the covariance between parameters. To minimize the covariance, S_X would be a diagonal matrix in which the off-diagonal terms would contain zeros. For this reason, P is defined to transform X such that the covariance matrix of Y is diagonalized.

$$S_Y = \frac{1}{n-1} YY^T$$

Rewriting S_Y in terms of X and P yields:

$$S_Y = \frac{1}{n-1}(PX)(PX)^T$$

$$S_Y = \frac{1}{n-1}PXX^TP^T$$

In the above equation, S_Y can be diagonalized by solving for P so that XX^T is diagonalized. If A is defined as $A = XX^T$, then A is a symmetric matrix and by definition it is orthogonally diagonalizable. This asserts that a diagonal matrix D exists such that A can be expressed as the following,

$$A = EDE^T$$

where E is an orthogonal matrix containing columns of orthonormal eigenvectors of A. By setting $P = E^T$, P now contains rows of eigenvectors of A and the following substitutions can be made.

$$A = P^TDP$$

$$S_Y = \frac{1}{n-1}PAP^T$$

$$S_Y = \frac{1}{n-1}P(P^TDP)P^T$$

$$S_Y = \frac{1}{n-1}(PP^T)D(PP^T)$$

Since P is orthogonal, $P^{-1} = P^T$.

$$S_Y = \frac{1}{n-1}D$$

The diagonal of S_Y contains the variances of the new parameters and the off-diagonal covariance terms are now zero. The principal components of *X* are the rows of *P*, or the eigenvectors of XX^T.

Referring back to the original equation where $PX = Y$, *Y* can be thought of as a projection of *X* along *P*. Since *P* is orthogonal, the cough parameters in *X* are projected along orthogonal eigenvectors in m-dimensinal space minimizing the covariance in *X*. The new cough parameters, *Y*, are essentially the sum of the orthogonal eigenvectors multiplied by the cough parameters. The degree of variance explained by each eigenvector corresponds to the diagonal terms of S_Y. The percent variance explained by each principal component can be calculated by dividing the variance corresponding to the respective principal component along the diagonal of S_Y by the sum of all the diagonal components of S_Y.

The principal components are ordered so that the first principal component is the eigenvector in the direction where the variance in *X* is maximized, and the last principal component is the eigenvector in the direction with the least variance. The actual number of principal components used in the transformation is dependent on the degree of explained variance desired by the user [42].

4.4.2 Neural Network

After performing a PCA on the training dataset, the resulting cough parameters were sent to a single neuron feed-forward back propagation neural network created using the Matlab Neural Network Toolbox. See Figure 4-12. The

back propagation algorithm is an iterative gradient descent algorithm designed to minimize the mean square error between the actual output and the desired output.

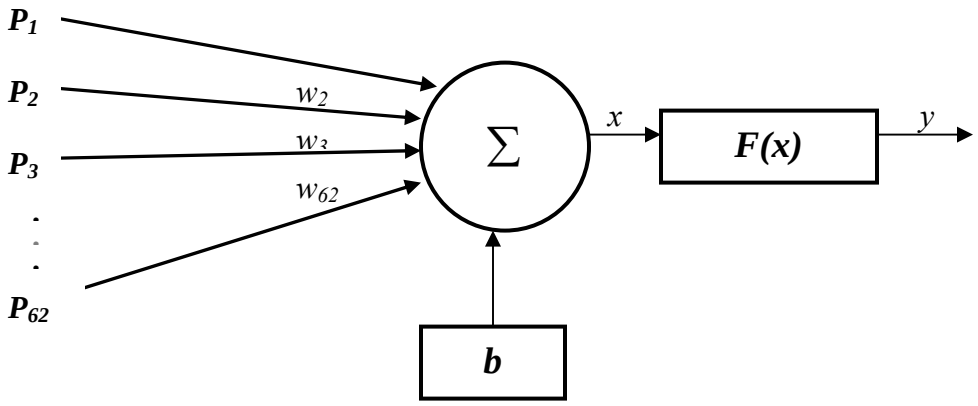

Figure 4-12 Cough Analysis Neural Network

In Figure 4-12, P_1 through P_{62} are the parameter values after PCA for a single cough. w_1 thourgh w_{62} make up the weight vector w, and b is a bias component added after the summation of the product of the parameter inputs and input weights. The output y is obtained from a bipolar sigmoid transfer function $F(x)$ defined as

$$F(x) = \frac{2}{(1+e^{-2x})} - 1$$

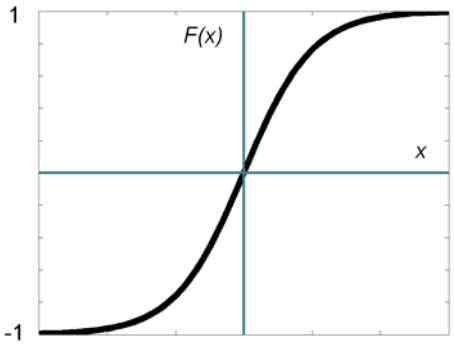

Figure 4-13 Bipolar Sigmoid Transfer Function

Coughs in groups 1, 2, and 3 were trained with target inputs $d = -1$, 0, and 1 respectively. The adaptation of the neuron weights and bias component are made using the following equations.

$$w(k+1) = w(k) - \alpha(k)g(k)p(k)$$
$$b(k+1) = b(k) - \alpha(k)g(k)$$

w(k) and *b(k)* are the present neuron weights and bias, *w(k+1)* and *b(k+1)* are the updated neuron weights and bias component, *α(k)* is the learning rate, *p(k)* is the input to the neuron and the gradient is defined as $g(k) = \frac{dF(x)}{d(x)}(d - y)$. The updates are made only after the entire training set has been applied to the network, constituting one complete epoch. The gradients calculated at each training example are added together to determine the change in the weights and bias. Neural network training is complete when one or more of the following criteria are met.

1) 200 training epochs were reached
2) The desired MSE has been met
3) The gradient vector is no longer being minimized

After training the neural network, the weights and bias component of the neural network were saved. The performance of the trained neural net can be evaluated by transforming the test dataset, using the principal component vectors obtained from the training set, and comparing the output of the neural network with the measured $R_{AW}C_G$ for the coughs in the test dataset.

Chapter 5 – Results and Discussion

This Chapter contains the results from the processing techniques explained in the previous chapter. The changes in the 128 derived cough parameter values from group 1 to group 3 will be used to indicate how the cough changes as the specific airway resistance increases by a factor of two. The completeness in how well the cough parameters describe the time and frequency content of the cough will be evaluated, and the validity of the model will be examined based on the ability to differentiate between coughs belonging to groups 1 and 3.

5.1 Acoustical Effects of the Head Chamber

Upon further observation of the results obtained from the cough power spectra and spectrograms, there were reasons to believe sound reverberations were present in the head chamber. The abrupt power changes in adjacent frequencies of the power spectrum in conjunction with the high-powered horizontal bands of the spectrograms may indicate that resonant frequencies of the head chamber were causing select frequencies to be amplified and remain present in the recorded cough sound.

To determine how the head chamber was affecting the cough sound properties, coughs were collected after insulating the inside of the chamber with sound absorbent foam. The effectiveness of the sound absorbent foam was evaluated by playing a 0 – 20kHz white noise signal into the insulated head chamber. The resulting white noise power spectrum was flat in the specified frequency range. An exposure was then conducted to record coughs inside the sound absorbent head chamber in the same fashion as previous cough sounds were obtained. The resulting

cough power spectrum, shown in Figure 5-1, was similar to the previously obtained power spectra. Power oscillations between adjacent frequencies are still evident in the spectrum, and three predominant power peaks occur near 2kHz, 8kHz, and 17kHz. Similar power spectrum characteristics were found in the previously gathered cough sounds. Unfortunately, direct comparison between the non-sound absorbent and sound absorbent head chamber cough spectra could not be made since no two coughs have identical power spectra.

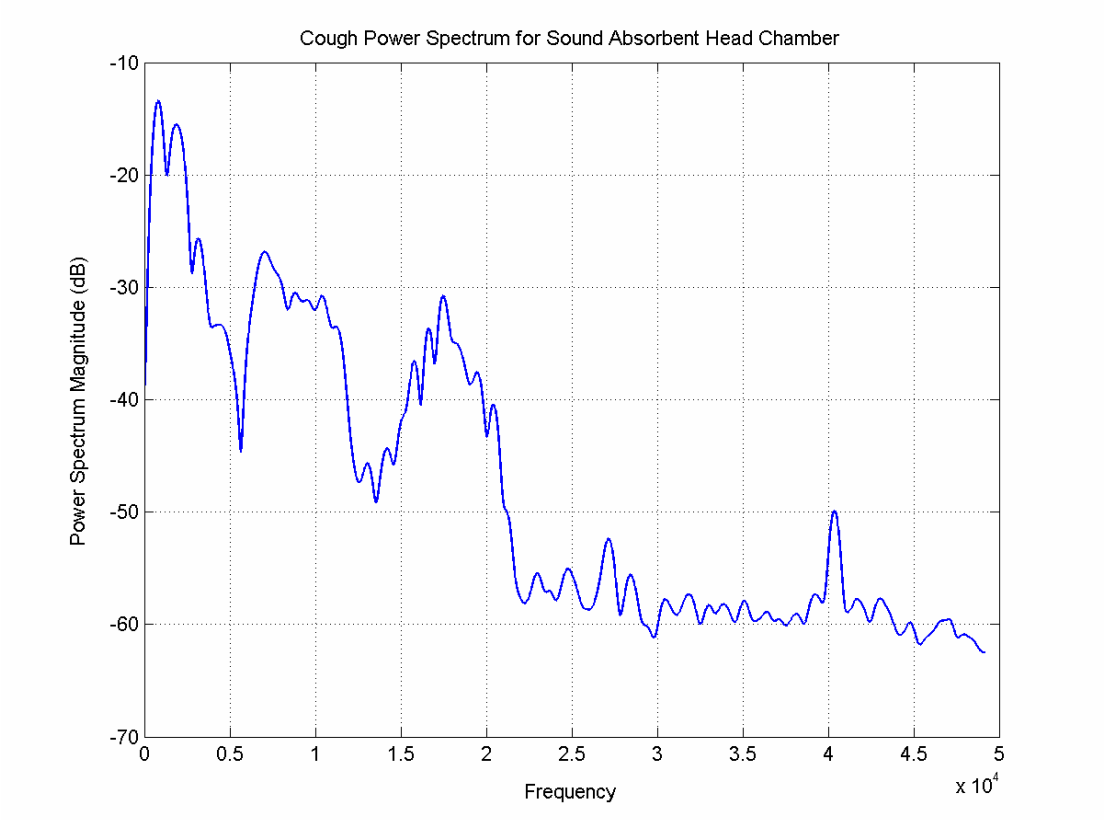

Figure 5-1 Cough Power Spectrum from Sound Absorbent Head Chamber

5.2 Cough Length

Cough lengths were fairly consistent between the two groups. See Table 5-1. Ideally, coughs would only be collected after a full inspiration to determine the effects of airway resistance on cough length. Unfortunately this stipulation could not be made since there was no way of forcing the animal to follow a developed cough maneuver protocol. With this limitation, cough length could not be considered a significant indicator of airway resistance. The cough length average, standard deviation, minimum, and maximum cough lengths support this assumption.

Table 5-1 Cough Length Statistics

Cough Length Statistics			
Group #	**Avg ± std (s)**	**Min (s)**	**Max (s)**
1	0.110 ± 0.023	0.048	0.16
3	0.109 ± 0.048	0.048	0.21

5.3 Acoustical Energy and Power

The following energy and power calculations were strictly based on the analysis of the electrical signal of the microphone as described in section 4.2.2. On average, there was a 48% decrease in energy and average power from the coughs in group 1 to group 3. See Figures 5-2 and 5-3.

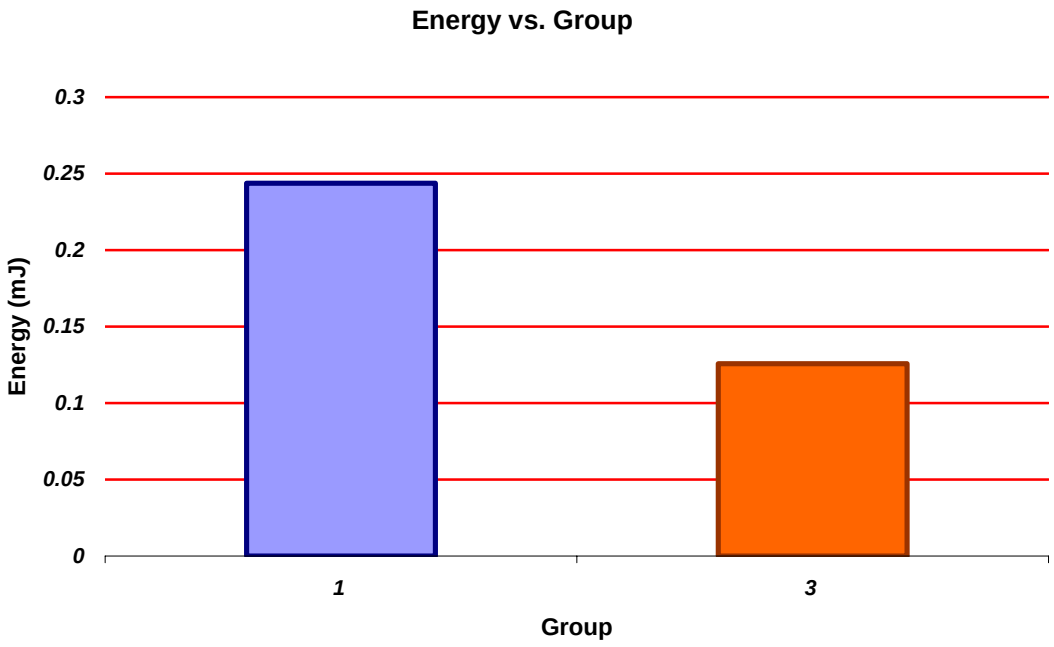

Figure 5-2 Energy vs. Cough Group

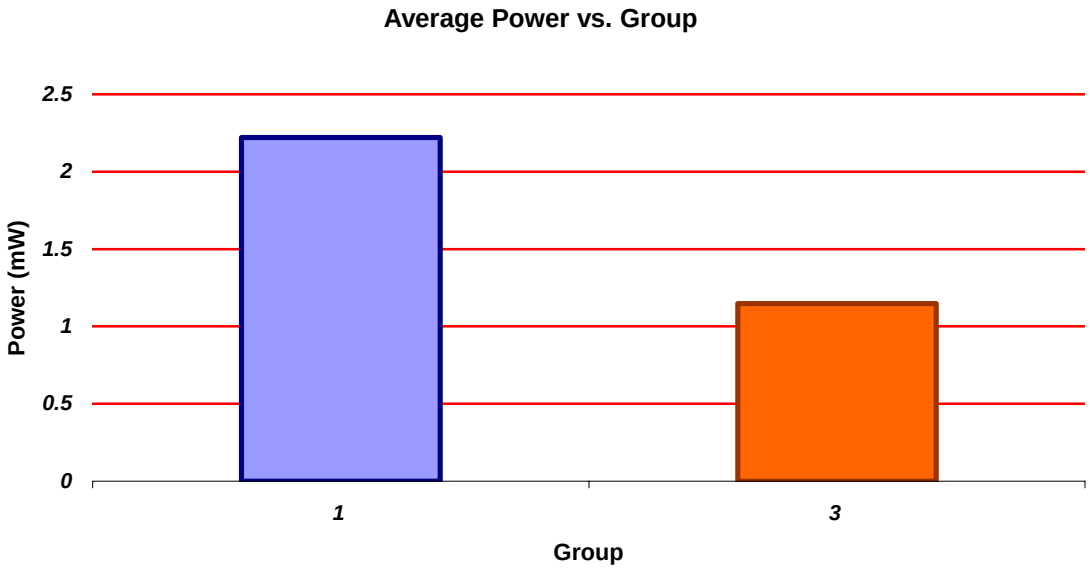

Figure 5-3 Average Power vs. Cough Group

As expected, based on the energy and average power measurements, the peak power measurements obtained from the power spectrum also indicate a significant decrease from group 1 to group 3. See Figure 5-4.

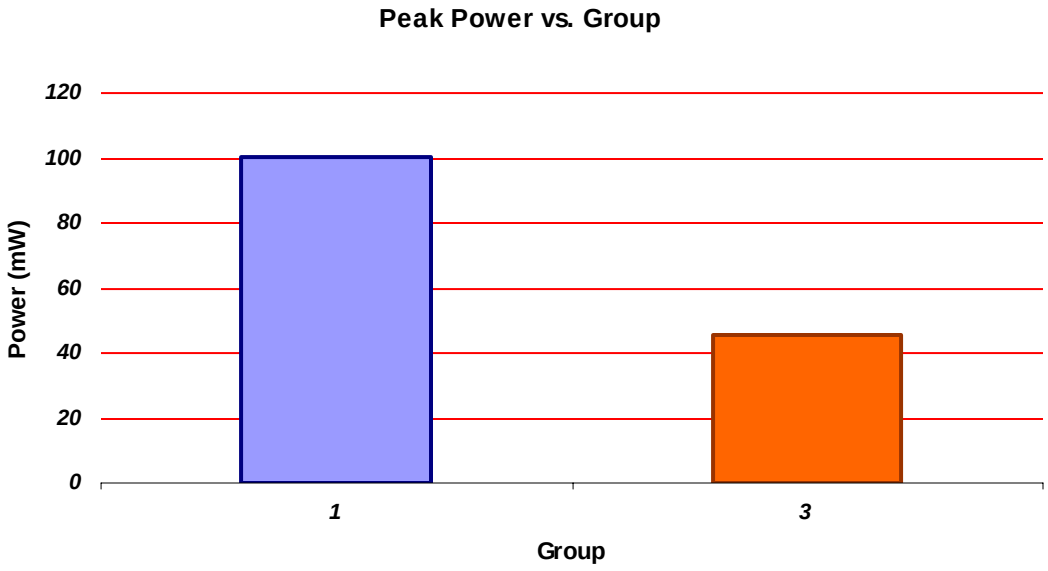

Figure 5-4 Peak Power vs. Group

In order to provide a reference to the loudness of the guinea pig cough, the peak and average sound pressure levels were calculated. The voltage signal from the microphone was attenuated by 40dB since a 40dB voltage gain was applied by the 2200C preamp/power supply during acquisition. The adjusted voltage signal was converted to microPascals using the $1.3V/10^6$ uPa sensitivity specification of the microphone. The peak and average sound pressures were obtained from the signal to calculate the sound pressure level, using the following equation [40].

$$SPL = 20\log\left(\frac{p}{p_o}\right) dB \text{ re } p_0$$

p is the sound pressure measurement, and p_0 is the reference pressure of 20 uPa. For coughs in group 1, the peak and average sound pressure levels were 52dB and 11.1dB. For coughs in group 3, the peak and average sound pressure levels were 50.9dB and 7.7dB. As a qualitative sound reference, 50db is equivalent to the sound level of an average home and 10dB is equivalent to the sound level of a rustling leaf.

5.4 Acoustical Frequency Characteristics

119 cough sound parameters were obtained based on the frequency content of the cough sound. The frequency dependent acoustical cough sound parameters were derived from the cough sound spectrum and the time dependent cough spectrograms.

5.4.1 Power Spectrum Analysis

Parameters were derived from the cough sound power spectrum using a combination of Welch's and Burg's power spectrum estimates. Since accoustical power and energy measurements were independently measured, percent of total power within the cough was used for measuring power spectrum parameters instead of the actual frequency power. The objective was to shift the focus from the decreased power found in the more restrictive coughs of group 3 and place an increased emphasis on how the shape of the power spectra were changing between the two groups.

In Figure 5-5 , the average power spectrum for group1 and group 3 are shown based on Burg's power spectrum estimate. The power spectrum is only plotted to 30kHz since 99% of the power is in this range. The average power spectrum was calculated by taking the mean percent power of each of the 32 equally sized frequency blocks for all the coughs in each group. The power spectrum shapes from group 1 and group 3 appear very similar. The discrepancies lie at two general locations. Group 3 cough spectrums appear to decrease from 10% of total power to 6% at approximately 750Hz and increase slightly in the 6000 – 11000Hz frequency band.

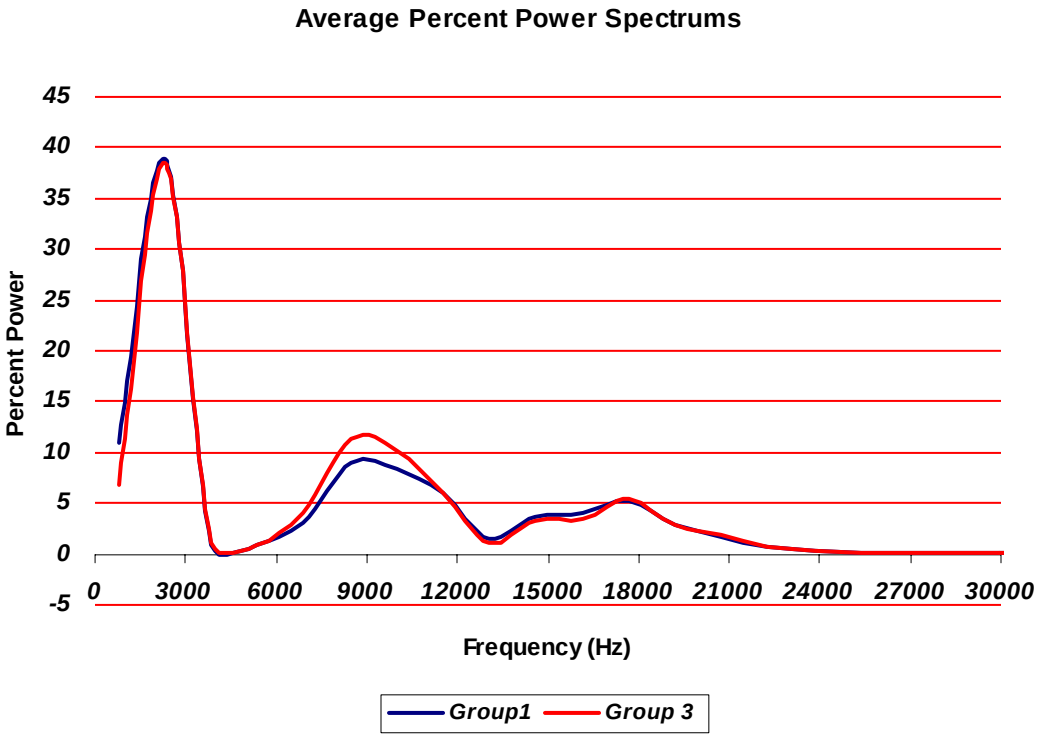

Figure 5-5 Burg's Average Percent Power Spectrum

Figure 5-5 suggests that the dominant frequencies are near 2200Hz for both groups. Dominant frequencies were recorded based on the frequency with the most power based on Welch's and Burg's power spectrum estimates. The dominant frequencies are shown for each power spectrum in Figures 5-6 and 5-7.

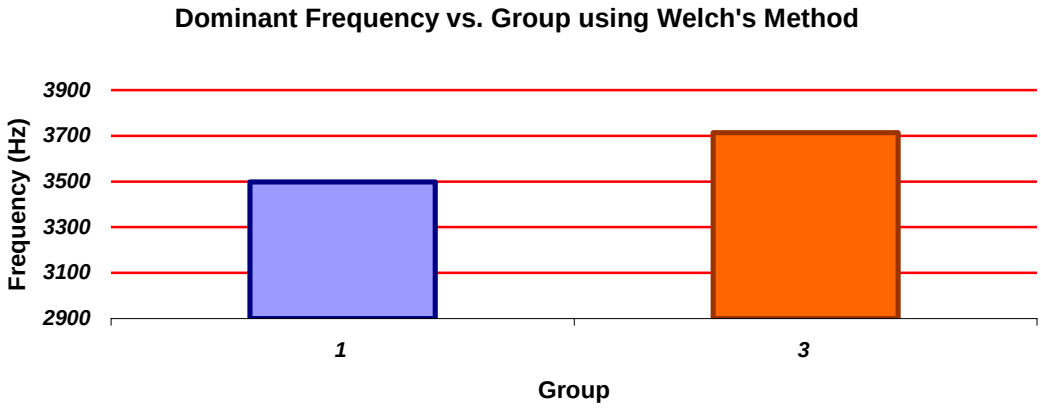

Figure 5-6 Dominant Frequency using Welch's Power Spectrum

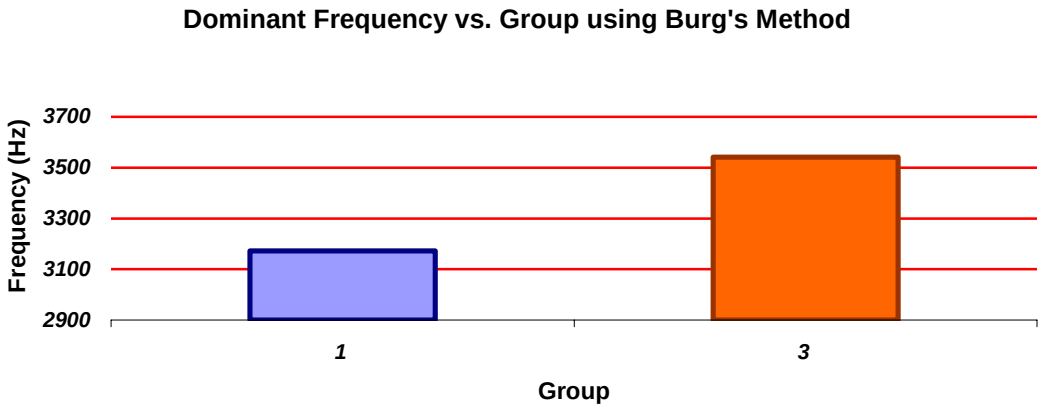

Figure 5-7 Dominant Frequency using Burg's Power Spectum

The dominant frequencies appear to be slightly higher than indicated by the average power spectrum in Figure 5-5. This can be attributed to the fact that 12.5% of coughs in group 1 and 17% of coughs in group 3 contained dominant frequencies greater than 3kHz. Upon examining the power spectrums and spectrograms in greater detail, the coughs having dominant frequencies greater than 3kHz had a pronounced wheeze in frequency bands greater than 3kHz causing the shift in dominant frequencies.

Another common acoustical analysis technique is an octave analyzer. Since an octave analyzer uses a nonlinear frequency scale, the information derived from the power spectrum could be more diversified. The octave analyzer used for analyzing the cough sound is defined by Table 5-2.

Table 5-2 Octave Frequency Breakdown

Octave	1	2	3	4	5	6	7
Frequency (kHz)	0.5 – 1	1 – 2	2 – 4	4 – 8	8 – 16	16 – 32	32 - 49

14 cough parameters were obtained from the following octave analysis using Welch's and Burg's power spectrum estimates. The results are shown in Figures 5-8 and 5-9.

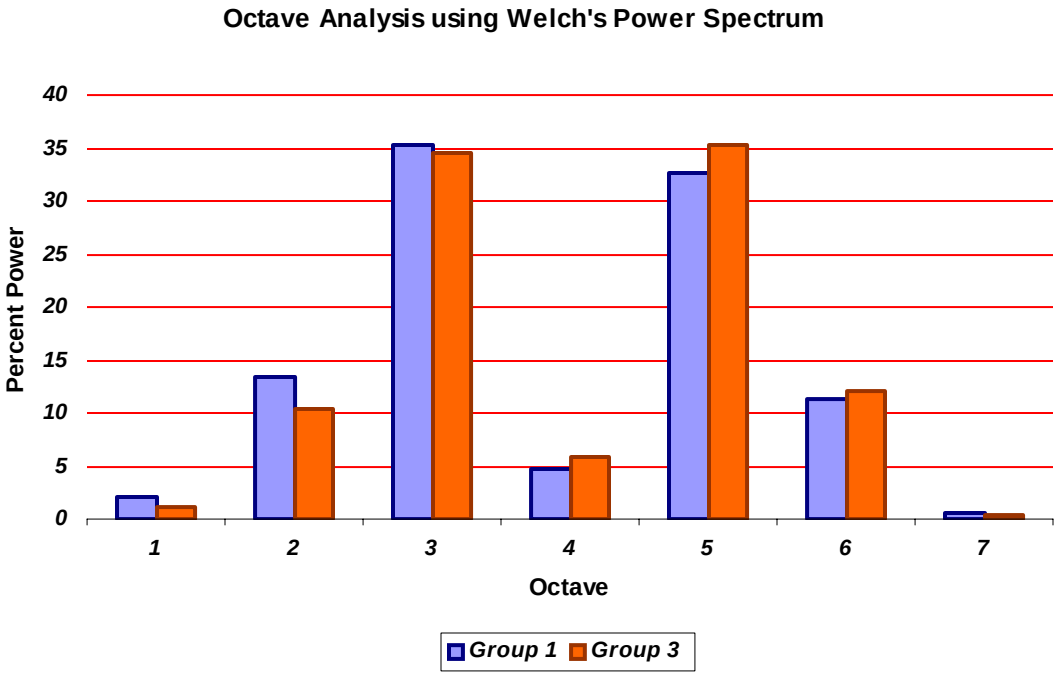

Figure 5-8 Octave Analysis using Welch's Power Spectrum

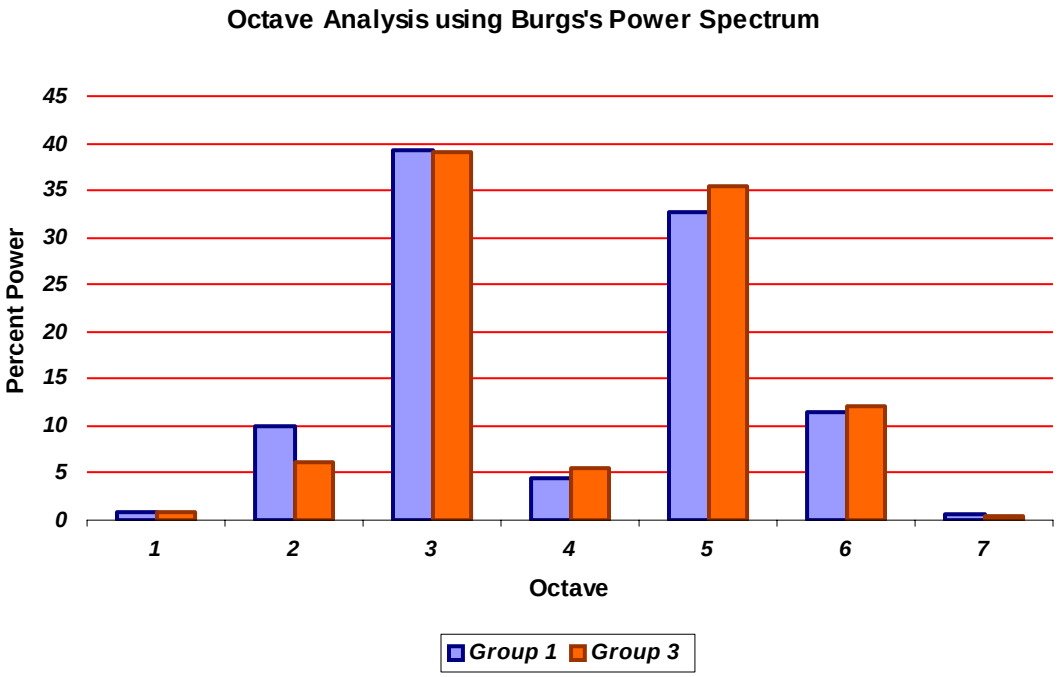

Figure 5-9 Octave Analysis using Welch's Power Spectrum

The results of the octave analysis are similar for both power spectrum estimation techniques. The percent powers in the first three octaves and the last octave are slightly lower in group 3. The power from these octaves appear to be transferred to octaves four through six. This indicates that coughs occurring during high airway resistances exhibit a higher percentage of power in the 4 – 32kHz frequency range. This does not suggest that coughs occurring at higher airway resistances have more power at higher frequencies. To illustrate this point consider the power spectra and octave analysis of a cough selected from group 1 and a cough selected and group 3. See Figures 5-10 and 5-11.

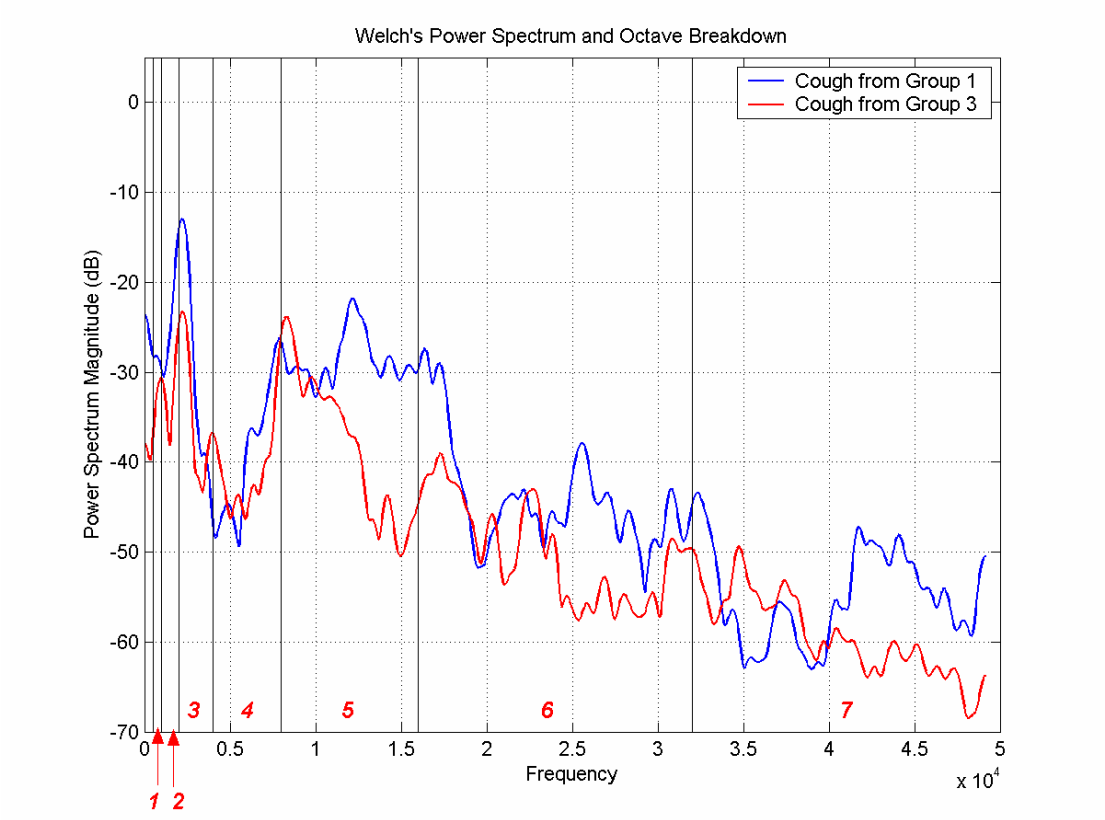

Figure 5-10 Power Spectrum Comparison for a Cough from Group 1 and a Cough from Group 3

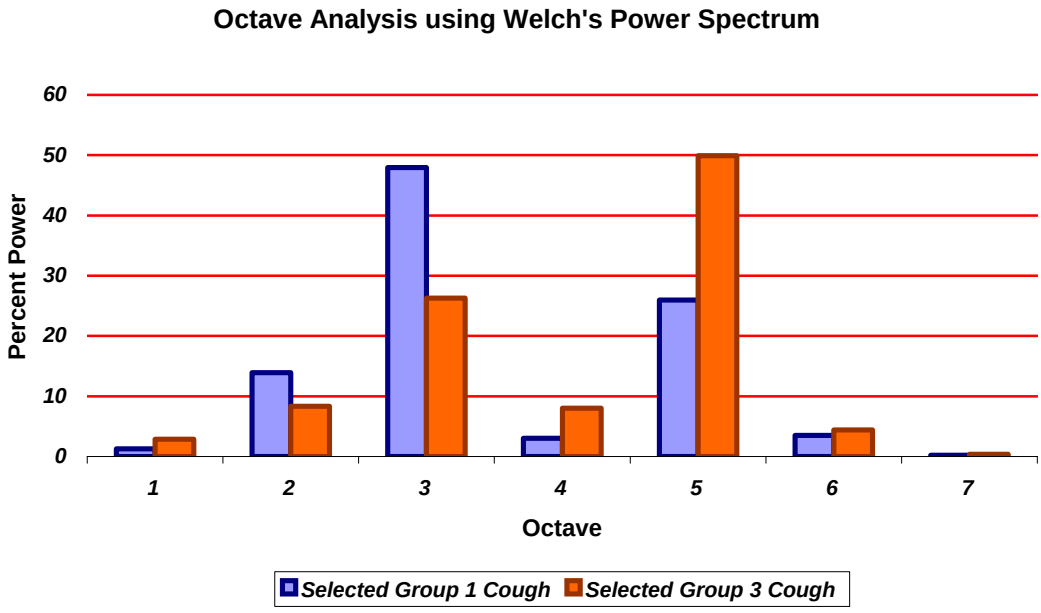

Figure 5-11 Octave Comparison for a Cough from Group 1 and a Cough from Group 3

Although the percent power in octaves four through six are higher for the cough from group 3, the power spectrum indicates that the total power is less in all octaves. The higher octaves contain a higher percentage of power in the cough from group 3 due to the decreased power in the lower octaves, particularly octaves two and three.

5.4.2 Spectrogram Estimate

The parameters derived from the cough sound spectrograms were used to quantify the frequency changes at different times within the cough. Dominant frequency, average frequency, and midpoint power in frequency bands represent 70 parameters obtained from the spectrograms. Since the cough lengths varied greatly within each group, parameters were derived based on time relative to the duration of the cough. In the dominant frequency plot, the cough was divided into ten time frames and the frequency containing the maximum power was recorded. The average

values for groups 1 and 3 can be viewed in Figure 5-12. The dominant frequencies in group 3 tend be slightly higher near the beginning of the cough. After reaching the third time division, the dominant frequencies gradually decrease in group 3 while the dominant frequencies in group 1 continue to increase slightly. This suggests that the higher frequencies tend to dissipate as time progresses in coughs occurring during increased airway constriction.

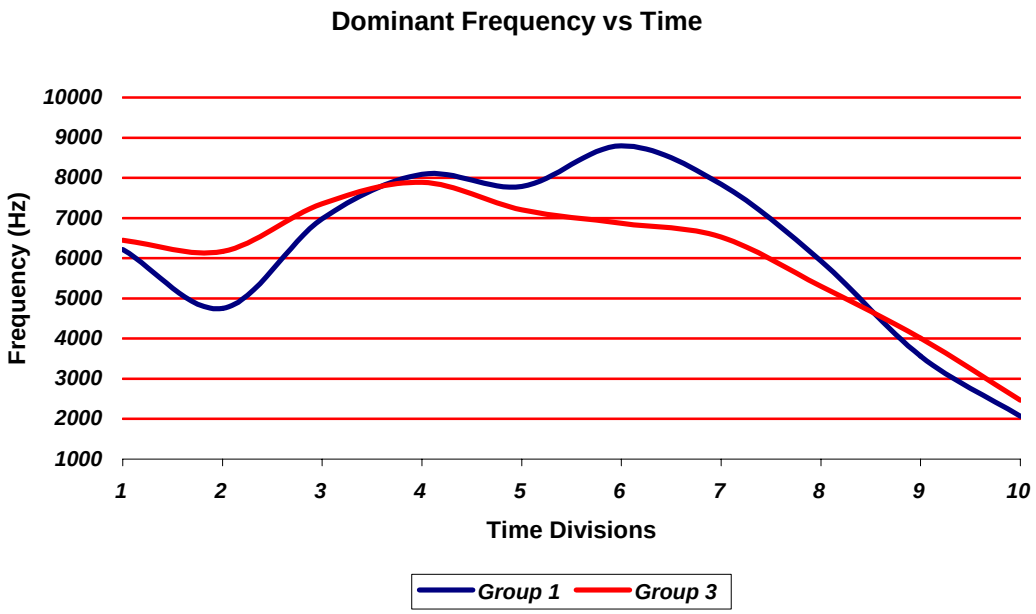

Figure 5-12 Dominant Frequency vs. Time

From the previously discussed power spectrum, the dominant frequency appeared to occur between 2 – 3kHz. The dominant frequencies found in the spectrogram are considerably higher. By studying the dominant frequency as a function of time, additional information is provided about the most powerful frequencies in the spectrum instead of an overall average approach of the power spectrum.

To further study how frequencies change during the cough, the average frequency of the spectrograms were calculated for each group. See Figure 5-13.

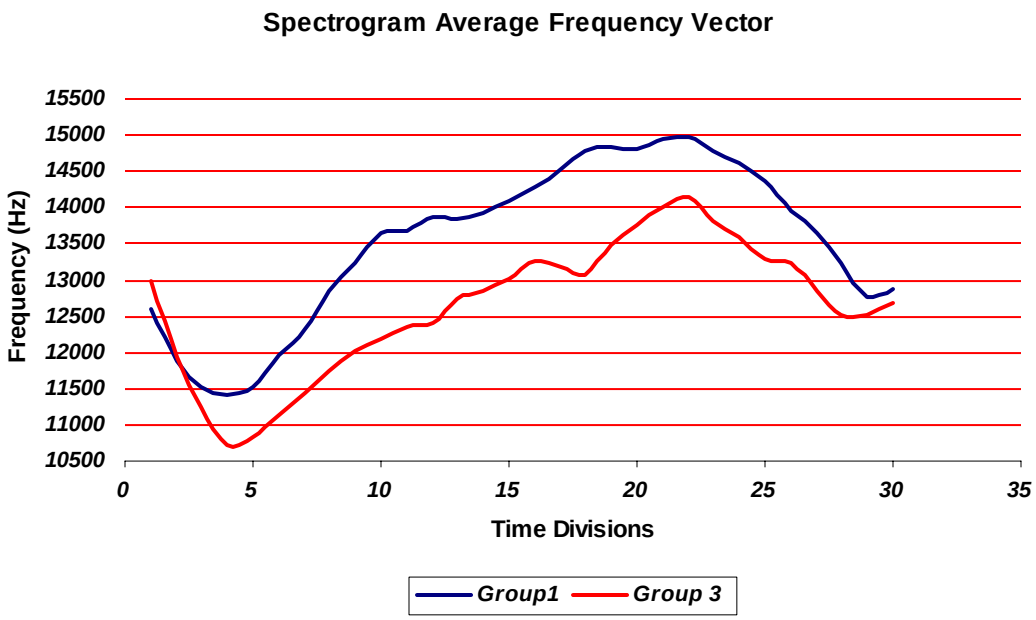

Figure 5-13 Average Frequency Comparison vs. Time

The average frequency vector shows how the shape of the spectrogram is changing by splitting the spectrogram horizontally based on the power weighted frequency averages. Interestingly, the shapes of the spectrograms from both groups are quite similar. The differences lie in the overall pitch of the coughs. During the start of the coughs in group 3, the average frequency is slightly higher and drops immediately after the initial cough sound. After the initial drop, the average frequencies are lower for coughs in group 3 indicating the power is more compressed into the lower frequencies of the group 3 coughs. To illustrate this point further, examine spectrograms in Figures 5-14 and 5-15. After 0.02 seconds the power in the selected group 3 cough is primarily limited to frequencies below 20kHz while frequencies up to 30kHz are present throughout the majority of the cough selected from group 1.

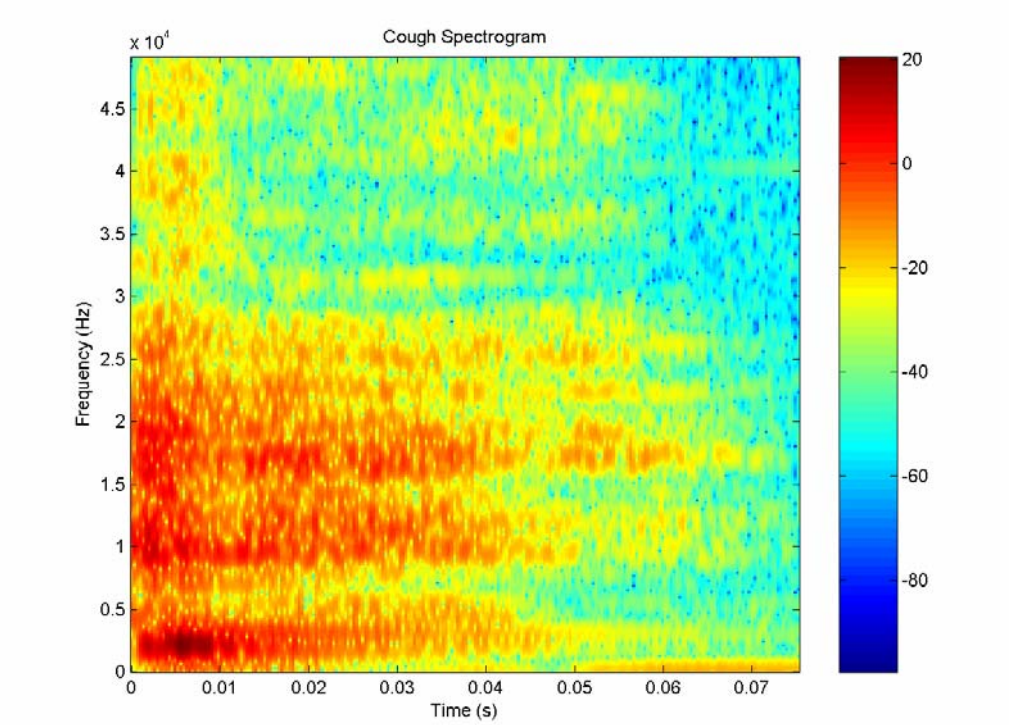

Figure 5-14 Group 1 Cough Spectrogram

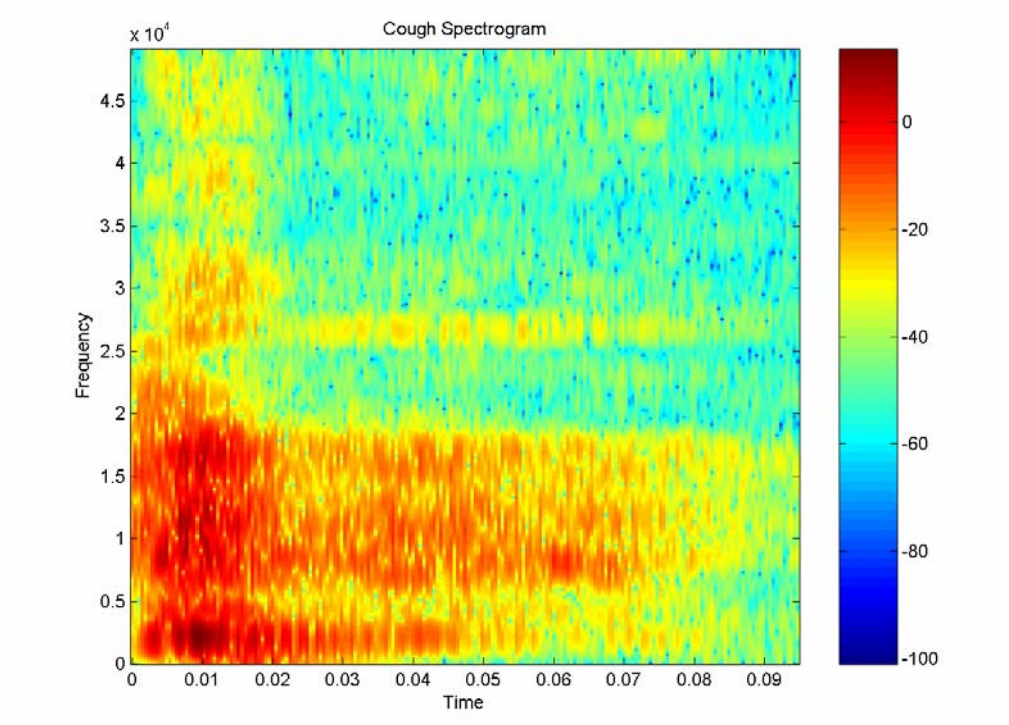

Figure 5-15 Group 3 Cough Spectrogram

The final group of parameters derived from the spectrogram are obtained from the time at which the midpoint power is met in 30 non-overlapping frequency bands. See Figure 5-16. The power midpoint comparison characterizes the horizontal changes visible in the spectrogram by finding the time into the cough where the midpoint of power is reached in the defined frequency bands.

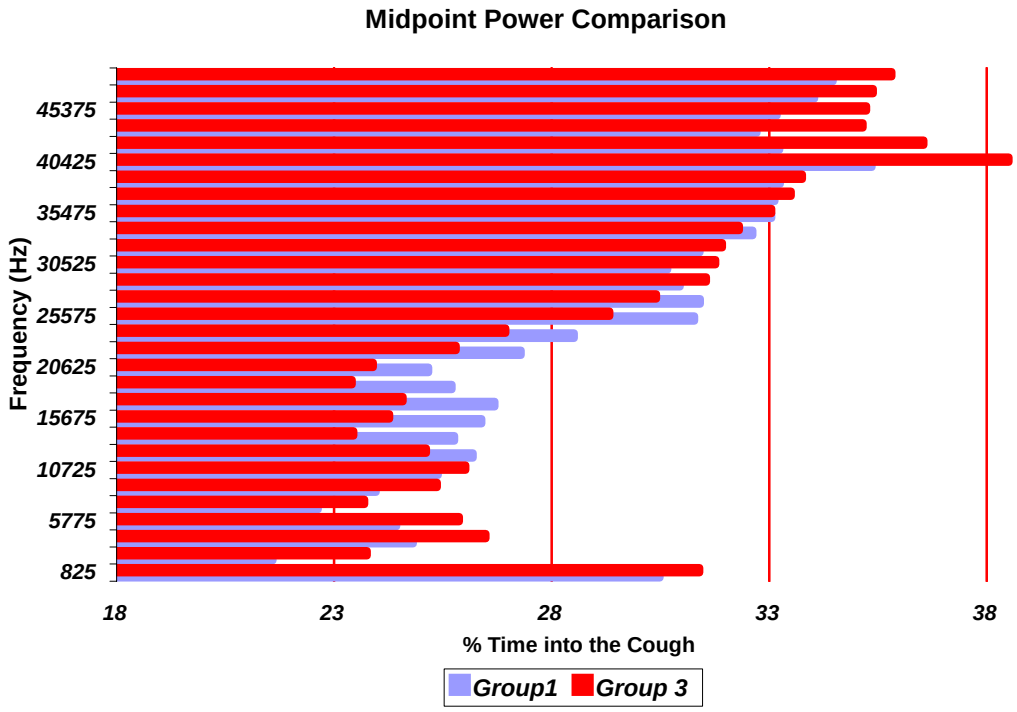

Figure 5-16 Midpoint Power Comparison

The power midpoint in the cough sounds can be affected by several factors. In the cough spectrograms, the cough signal starts predominantly as a broadband frequency signal. After the initial broadband output, certain frequency bands tend to remain in the cough. The frequencies that tend to dissipate first or frequencies containing the majority of the power in the beginning of the cough will cause the horizontal bars to shorten, while remaining frequencies containing equal power throughout the cough will cause the bars to lengthen. Another scenario is for

frequencies to appear at the end the cough that were not present at the beginning, this will cause the bars to lengthen as well. In cough sounds, this final case does not seem to be representative of what is actually happening.

Considering the aforementioned cases and the results illustrated in Figure 5-16, the following conclusions were made. Coughs in group 3 tend to have more power at the end of the cough in the 800Hz – 10kHz range illustrated by the longer midpoint power bars. In the 10 – 30kHz range, the longer blue bars associated with the coughs in group 1 indicate a more consistent power throughout the cough at those frequencies. The blue bars for group 1 coughs are shorter at frequencies greater than 35kHz since there is more initial power at those frequencies than in group 3 coughs.

5.5 Flow Analysis

Peak flow, average flow, peak acceleratory flow, and total expiratory volume parameters were calculated for all coughs using the methods described in section 4.3. The cough flow measurement techniques provided inaccurate flow measurements, making it impossible to deduce valuable information for the cough flow data. Therefore, they were not included in the analysis. The majority of the inaccuracy of the measurements can be attributed to two causes. In the time immediately proceeding and during the cough, the guinea pigs become increasingly agitated and increase their movement inside the plythesmograph. The increased movement causes the neck seal separating the head and thorax chamber to move. Due to the movement in the neck seal, the pressure signals in the chambers oscillate resulting in distorted cough flow measurements. The second cause is due to the flow frequency response of the head chamber. If cough flow is assumed to last the length of the cough sound,

then the duration of expired air exiting the mouth of the guinea pig is very short, approximately $1/10^{th}$ of a second. The short duration of increased flow being expired from the mouth of the guinea pig in conjunction with the capacitance created by the relatively large volume of the head chamber provided a poor cough flow frequency response.

5.6 Cough Characteristics versus Airway Resistance

From the results of previously described cough sound and flow analysis, 124 cough sound parameters were used in classifying coughs. Cough parameters obtained from the training dataset were analyzed using principal component analysis (PCA). The number of principal component vectors to be used in the analysis was based on the classification accuracy of the neural net. The best results were obtained using the first 62 principal components. The covariance matrix indicated the selected principal components accounted for 99.5% of the variability in the dataset. PCA enabled the cough parameter dimensions to be reduced by half while accounting for over 99% of the variability in the measurements. To obtain the new cough parameters for training and test datasets, the original parameters were multiplied by the principal component vectors.

The new cough parameters from the train dataset were then submitted to the neural net to appropriately weight the new cough parameters. A neural net was trained with and without the coughs from group 2. The neural net trained without the coughs from group 2 provided excellent results for the training set but decreased accuracy in classifying coughs from groups 1 and 3 in the test set. For this analysis,

coughs from group 2 were included in the training to provide the best overall separation between groups 1 and 3.

Coughs from groups 1, 2, and 3 were trained with target outputs of –1, 0, and 1 respectively. The training results are represented in Figure 5-17 as a cumulative distribution plot. The cumulative distribution plot tells the probability of having a cough in any group below a selected neural net output. It also provides a visual index to how well the neural net separated the coughs.

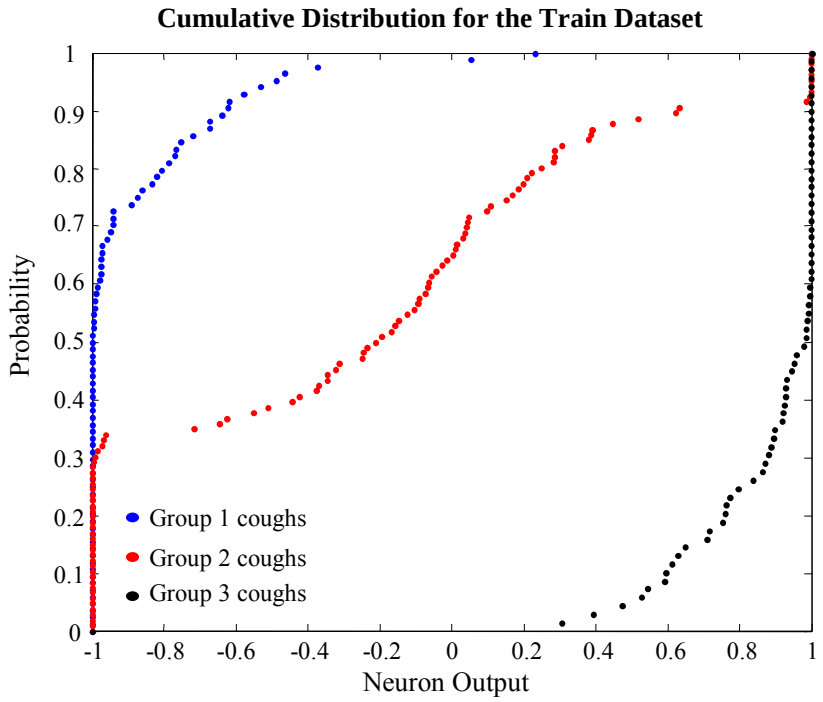

Figure 5-17 Cumulative Distribution Plot for Train Dataset

Using the principal component vectors and the neural net weights generated from the train dataset, the following results were obtained for the test dataset. See Figure 5-18.

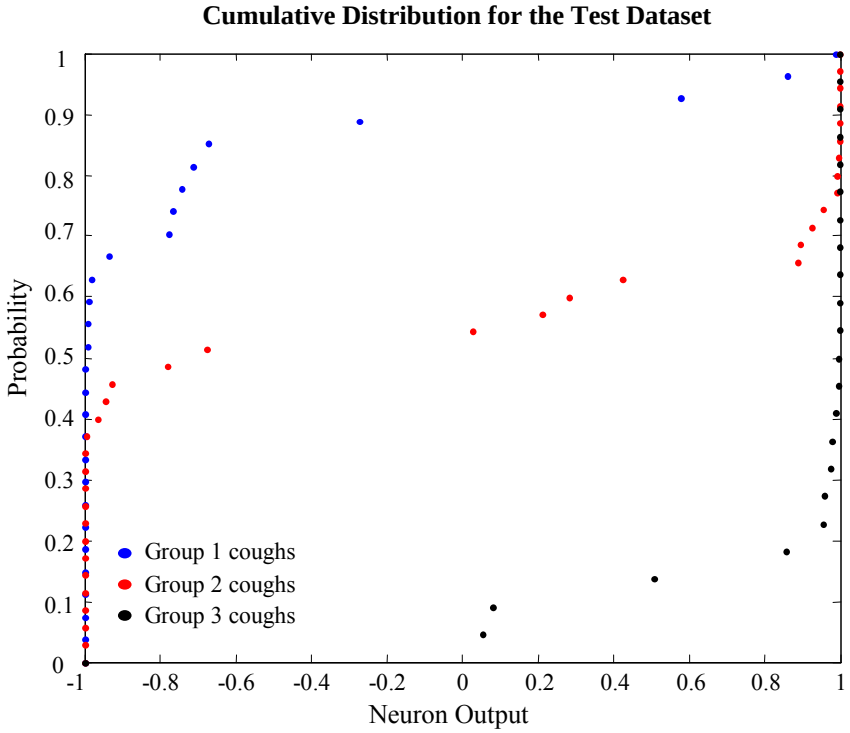

Figure 5-18 Cumulative Distribution for Test Dataset

The cumulative distributions for the train and test datasets show significant separation in coughs occurring in groups 1 and 3. The transition group, group 2, spans the range of the neuron output. This was expected given that group 2 represents coughs occurring between the airway resistance ranges specified by groups 1 and 3.

Since the focus of this analysis is to design a classification system capable of distinguishing coughs occurring during times of low airway resistance from coughs occurring during high airway resistances, a Receiver Operating Characteristic (ROC) curve was created to determine the accuracy and cutoff for separating the two groups. An ROC analysis provides a more comprehensive evaluation of the neural network

output and illustrates the cost/benefit relationship as a result of choosing different decision making criteria. See Figure 5-19.

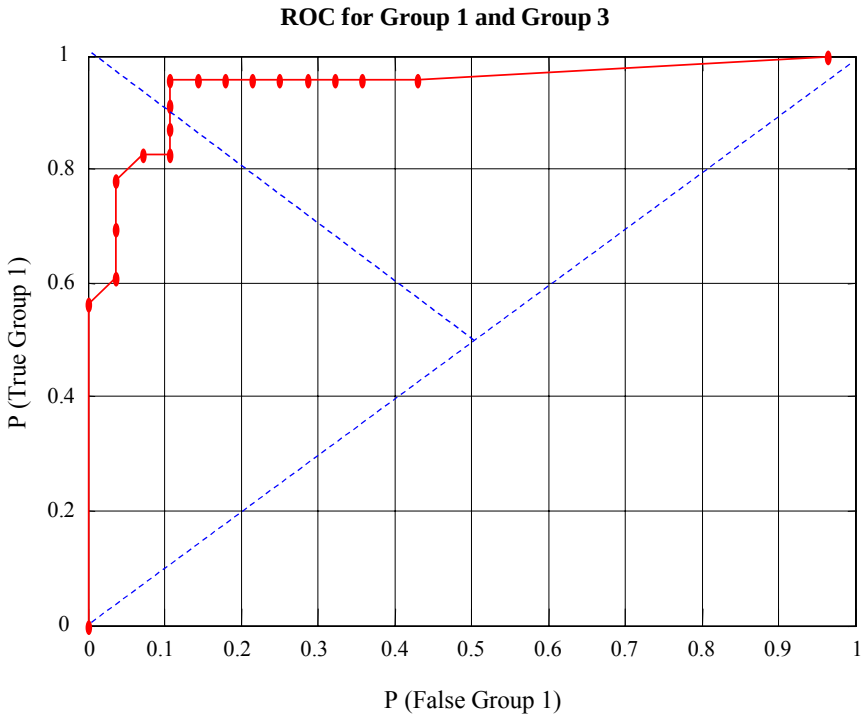

Figure 5-19 Group 1 and Group 3 ROC Curve for Test Dataset

P(True Group 1) is the probability of accurately classifying a cough into group 1, and P(False Group 1) is the probability of classifying a cough as group 1 when the cough belongs in group 3. An ROC curve can be described by three parameters. The first parameter is accuracy or the area under the curve. The area under the curve is the overall ability of the cough analysis to correctly classify coughs into group 1 and group 3. The second parameter is sensitivity, which measures the percent of accurate group 1 classifications. The final parameter, specificity, measures the percent of accurate group 3 classifications. Sensitivity and specificity are inversely related and the decision threshold can be adjusted to favor sensitivity or specificity. The accuracy of the ROC curve is 0.946 with equal sensitivity and specificity at 0.893.

Chapter 6 – Conclusions and Future Recommendations

6.1 Conclusions

This thesis has displayed the engineering process involved in this area of research up to this point; including the primary concept and motivation, through the equipment selection and calibration, the signal processing of the acquired cough sounds, to the cough classification algorithm. The goal of designing an exposure system that can be used to collect acoustical information within a guinea pig cough and depict changes in the acoustical properties at low and high levels of chemically induced airway resistance has been accomplished. Flow measurements and analysis are still unrefined.

A large number of parameters were developed for the acoustical cough characterization due to the variability in cough length, differences in cough sounds between guinea pigs, and the lack of initial knowledge as to how the cough sound would change with respect to airway resistance. Based on the results of the analysis, the developed cough parameters appear to provide significant information to how the cough sound changed from low to high levels of chemically induced airway resistance. Since many cough parameters may reflect similar information about the cough, principal component analysis provided a way to effectively reduce the redundancy in the parameters.

The animal cough model shows that changes in the acoustical characteristics of the guinea pig cough can be used to reflect alterations in pulmonary function. Accurately characterizing the cough sound and diagnosing guinea pigs with

significantly increased airway resistance is the first step in analyzing the effects of other pulmonary irritants on cough sound.

6.2 Future Recommendations

While the present work on this project has provided valuable results, there are a number of methods considered paramount to the success of future iterations of this design and process. Numerous other signal processing techniques can be applied to extract more information from the cough sound and form new cough parameters. Sound reverberations present in the head chamber need to be addressed from a signal processing standpoint or through a redesign of the head chamber. From a comparative perspective, reverberations caused by the head chamber are negligible. In order to accurately characterize the cough sound, reverberations must be attenuated.

A more accurate way to measure cough flow is also needed. Reducing the volume of the head chamber may help with the inadequate flow frequency response, but animal movement during the cough would also need to be considered. The head chamber could be modified in a way to restrain head movement during the cough.

Upon addressing the aforementioned issues, additional exposures are needed to validate the findings supported in this thesis. The use of bronchodilating chemicals to induce cough would extend the range of airway measurements and further enhance the study. It would also be interesting to conduct and compare the results from a similar study based on the coughs from a single animal, providing enough coughs with varying airway resistances could be gathered.

The next phase of research would be to compare cough flow and acoustical characteristics before and after exposures to common occupational pulmonary irritants. Changes in guinea pig cough characteristics could then be compared to known changes found in human cough characteristics. The validity of the animal cough model could then be examined in more detail.

Appendix A – Complete Hardware Specifications

MASS AIRFLOW CONTROLLERS

Use	Nebulized Airflow Controller	Dilutant Airflow Controller
Part No.	GFC1735	G20589C
Flow Range	0 – 5 L/min	0 – 10 L/m
Max Input Pressure	500 psig (34.5 bars)	500 psig (34.5 bars)
Leak Integrity	1 x 10^{-7} of helium	1 x 10^{-7} of helium
Setpoint Control	Local or remote	Local or remote
Analog out	0-5 Vdc and 4-20 mA	0-5 Vdc and 4-20 mA
Other Specs.	• NIST traceable certification • circuit protection • totalizer option	

SETRA PRESSURE TRANSDUCER SPECIFICATIONS

Full Scale Pressure Output	**Model 239 (Voltage):** Bi-directional: ±2.5 VDC
Zero Pressure Output	0 VDC
Accuracy (RSS Method)	±0.14% Full Scale
Type of Pressure	Differential
Pressure Ranges	Bi-directional: 0 to ±0.25 in. WC
Thermal Effects	Compensated Range °F (°C): 30 to 150 (-1 to 65) %FS/100°F(100°C)max.zero: ±1.0 (±1.8) %FS/100°F(100°C)max.span: ±1.0 (±1.8)
Media	Positive Pressure: Gases or liquid compatible with stainless steel, hard anodized 6061 aluminum (Buna N "O" Ring). Reference Pressure: Clean dry air or other gases (Non-corrosive, non-condensable).
Excitation Voltage	22-30V DC

AUDIO SPECIFICATIONS

Microphone

Model Number		**2530**
Nominal Diameter (inches)		1/4
Directive Characteristics		Random incidence & pressure
Frequency Response		4 Hz to 80 kHz
Nominal Open Circuit Sensitivity	*mV/Pa*	1.3
	dB rel. 1V/Pa	-57.7
Lower Limiting Frequency (Hz)		0.2 to 2
Open Circuit Distortion Limit 3% (dB rel. 20 µPa)		>172
Nominal Cartridge Thermal Noise [dB(A)]		31
Resonant Freq. (kHz)		80
Polarization Voltage (Vdc)		200

Preamplifier

Model	**PRM910B**
ICP Preamplifier	PRM422
Size	1/4 in
Power	Dual ± 10 to ± 18 V Single 20 to 35 V
Output Connector	5-pin Switchcraft®
Cable	6 ft, Integral cable

AUDIO SPECIFICATIONS (CONT.)

Power Supply

Bandwidth/Response **Lower limiting frequency as function of gain setting**		
Gain (dB)	**-3 dB Point (Hz)**	**-2 dB Point (Hz)**
0	0.2	1.0
10	0.4	2.0
20	1.6	81.0
Upper limiting frequency as function of output voltage (flat output)		
Output Voltage RMS	**-3 dB Point (Hz)**	
10.0	50K	
5.0	100K	
2.0	250K	
1.0	500K	
0.5	1M	
Signal Input (each channel)		
Gain	0 to 40 dB in 10 dB steps	
Attenuation	0 to 30 dB in 10 dB steps plus 22-turn vernier attenuator providing 0 to 10.4 dB continuous range.	
Bias Voltage	0, 28, 100, 200 Vdc, ±0.5% stability	
Input Impedance	20 kOhms @ 0 dB attenuation 70 kOhms @ 10 dB attenduation	
Crosstalk	80 dB to 20 kHz 60 dB to 200 kHz	
Connector Type	Switchcraft miniature XLR 5-pin (part no. TB4M) Cable requires TA5F connector	
Overload	10 V rms	
Signal Output (each channel)		
Impedance	50 Ohms	
Output Noise (dB reference 1 µV)		
Gain (dB)	**Flat (dB) (1 Hz - 20 kKz)**	**A-weight (dB)**	**C-Weight (dB)**
0	8.3 (2.6 µV)	0 (1 µV)	3.4 (1.5 µV)
40	35.3 (58.2 µV)	32.2 (40.7 µV)	30.9 (35.2 µV)

DAQ SYSTEM SPECIFICATIONS

NI 6036E DAQ Card

Analog Input	16 SE/8 DI
Input Resolution	16 bits
Max Sampling Rate	200 kS/s
Input Range	±0.05 to ±10 V
Analog Outputs	2
Output Resolution	16 bits
Output Rate	10 kS/s
Output Range	±10 V
Digital I/O	8
Counter/Timers	2, 24-bit
Triggers	Digital
Measurement Sensitivity (mV)	0.0036

DAQ SYSTEM SPECIFICATIONS (CONT.)

SCC 2345 Signal Conditioning Box

GENERAL SPECIFICATIONS	
16 analog inputs	Measurement type and connectivity selectable on a per-channel basis
8 digital I/O lines	Low-profile carriers for portable, rack-mount, and desktop applications
2 unconditioned counter/timers	Low-profile carriers for portable, rack-mount, and desktop applications
NI-DAQ driver software simplifies configuration, measurement, and scaling	
SENSOR/SIGNALS	
Thermocouples	Frequency input
RTDs	Lowpass filtering
Strain gauges	Isolated voltage/current output
Force/load/torque/pressure sensors	Isolated digital I/O
IEPE accelerometers	Relay switching
Isolated voltage/current input	
CONNECTIVITY OPTIONS	
BNC	SMB
Minithermocouple	Momentary pushbutton switch
Thermocouple	Rocker switch
LEMO (B-series)	Toggle switch
MIL-Spec	LED
9-pin D-Sub	Potentiometer
Banana jack	Strain relief

NI PCI-4451 DAQ Card

GENERAL SPECIFICATIONS	
Analog Input	2
Input Resolution	16 bits
Max Sampling Rate	204.8 kS/s
Input Range	±10mV to ±42.4 V
Analog Outputs	2
Output Resolution	16 bits
Output Rate	51.2 kS/s
Output Range	±10mV to 10V
Digital I/O	8
Triggering	Analog/Digital
DYNAMIC CHARACTERISTICS	
Alias-free Bandwidth	DC to 0.464 fs
Alias Rejection	80 dB, 0.536 fs < $f$in < 63.464 fs
Spurious-free Dynamic Range	90 dB
THD	-80 dB; -90 dB for $f$in < 20 kHz
IMD	-100 dB (CCIF 14 kHz + 15 kHz)
Crosstalk (Channel Seperation)	-100 dB, DC to 100 kHz

Appendix B – Airway Resistance Circuit Analysis

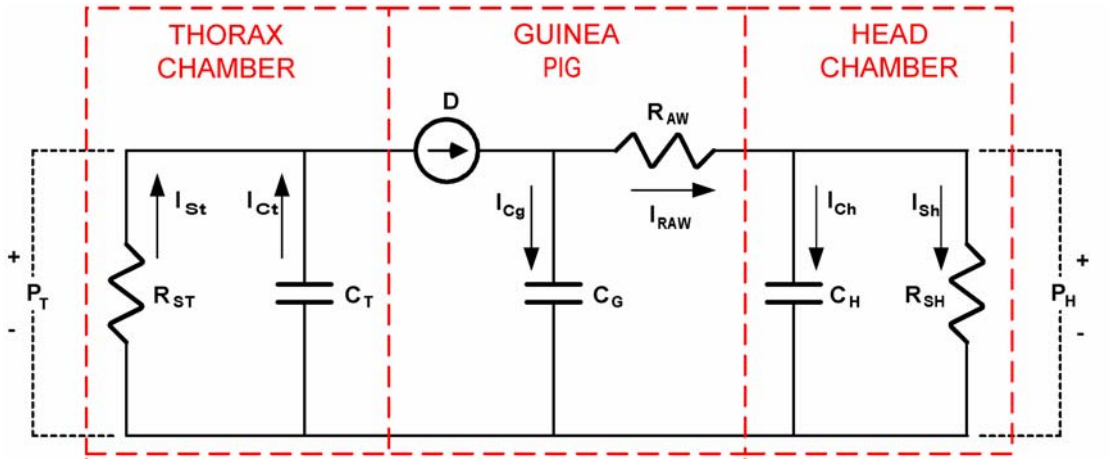

Let $P_T = u$

$P_H = y$

KCL $$D = i_{RAW} + i_{CG} \tag{1}$$

$$D = \frac{u}{R_{ST}} + i_{CT} = \frac{u}{R_{ST}} + C_T \frac{dV_{CT}}{dt} = \frac{u}{R_{ST}} + C_T \frac{du}{dt} \tag{2}$$

$$i_{RAW} = i_{CH} + i_{RSH} = C_H \frac{dV_{CH}}{dt} + \frac{y}{R_{SH}} = C_H \frac{dy}{dt} + \frac{y}{R_{SH}} \tag{3}$$

$$i_{CG} = C_G \frac{dV_{CG}}{dt} \tag{4}$$

$$V_{CG} = V_{RAW} + y = i_{RAW} R_{AW} + y \tag{5}$$

combining equations 3 and 5

$$V_{CG} = R_{AW}\left(C_H \frac{dy}{dt} + \frac{y}{R_{SH}} \right) + y \tag{6}$$

combining equations 4 and 6

$$i_{CG} = C_G \frac{d}{dt}\left(R_{AW}\left(C_H \frac{dy}{dt} + \frac{y}{R_{SH}} \right) + y \right) \tag{7}$$

substituting equations 2, 3, and 7 into equation 1 yields

$$\frac{u}{R_{ST}} + C_T \frac{du}{dt} = C_H \frac{dy}{dt} + \frac{y}{R_{SH}} + i_{CG} + C_G \frac{d}{dt}\left(R_{AW}\left(C_H \frac{dy}{dt} + \frac{y}{R_{SH}} \right) + y \right) \tag{8}$$

$$\frac{u}{R_{ST}} + C_T \frac{du}{dt} = C_H \frac{dy}{dt} + \frac{y}{R_{SH}} + i_{CG} + R_{AW} C_G C_H \frac{d^2 y}{dt^2} + \frac{R_{AW} C_G}{R_{SH}} \frac{dy}{dt} + C_G \frac{dy}{dt} \tag{9}$$

Laplace of equation 9

$$\frac{U}{R_{ST}} + C_T Us = C_H Ys + \frac{Y}{R_{SH}} + i_{CG} + R_{AW} C_G C_H Ys^2 + \frac{R_{AW} C_G}{R_{SH}} Ys + C_G Ys \tag{10}$$

$$U\left(\frac{1}{R_{ST}} + C_T s \right) = \left(C_H s + \frac{1}{R_{SH}} + i_{CG} + R_{AW} C_G C_H s^2 + \frac{R_{AW} C_G}{R_{SH}} s + C_G s \right) Y \tag{11}$$

$$U\left(\frac{1}{R_{ST}} + C_T s \right) = \left[\left(C_H s + \frac{1}{R_{SH}} \right) + i_{CG} + R_{AW} C_G s \left(C_H s + \frac{1}{R_{SH}} \right) + C_G s \right] Y \tag{12}$$

$$U\left(\frac{R_{ST} C_T s + 1}{R_{ST}} \right) = \left[\left(\frac{R_{SH} C_H s + 1}{R_{SH}} \right) + i_{CG} + R_{AW} C_G s \left(\frac{R_{SH} C_H s + 1}{R_{SH}} \right) + C_G s \right] Y \tag{13}$$

$$\frac{R_{ST}}{R_{ST} C_T s + 1} = Z_T \tag{14}$$

$$\frac{R_{SH}}{R_{SH} C_H s + 1} = Z_H \tag{15}$$

The circuit can then be simplified and rewritten as

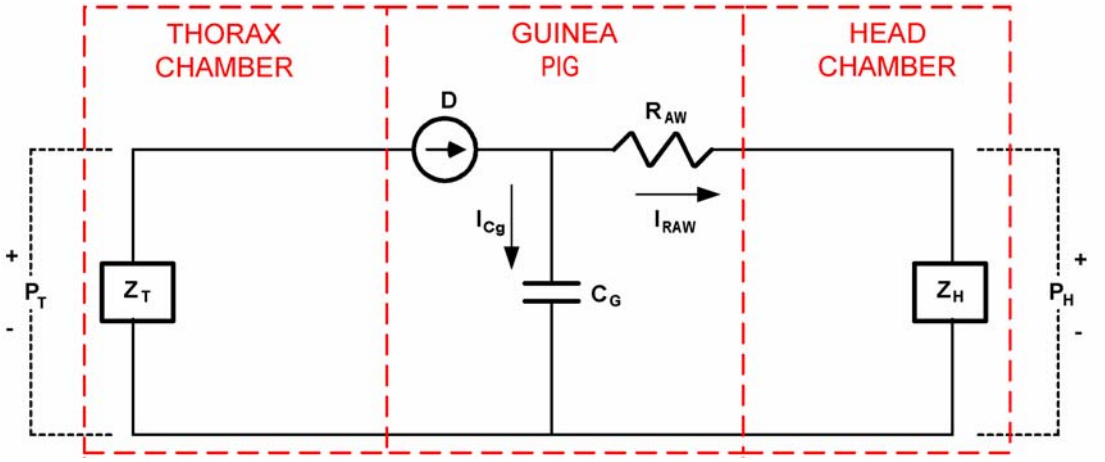

substituting equations 14 and 15 into equation 13 yields

$$U\left(\frac{1}{Z_T}\right)=\left[\left(\frac{1}{Z_H}\right)+i_{CG}+R_{AW}C_G s\left(\frac{1}{Z_H}\right)+C_G s\right]Y \tag{16}$$

$$\frac{U}{Z_T}=\frac{\left(R_{AW}C_G s+1+C_G Z_H s\right)Y}{Z_H} \tag{17}$$

$$\frac{Y}{U}=\frac{Z_H \big/ Z_T}{R_{AW}C_G s+1+C_G Z_H s} \tag{18}$$

$$\frac{Y}{U}=\frac{Z_H \big/ Z_T}{C_G\left(R_{AW}+Z_H\right)s+1} \tag{19}$$

References

1. Korpas J., and Tomori Z. *Cough and other Respiratory reflexes*. In: Herzog E S ed. Progress in Respiration Research. Basel: Karger, 1979: 15-179

2. Fuller RW. Cough. In: *Respiratory Medicine,* 2nd edition, Ed. Brewis RAL, Corrin B, Geddes DM, Gibson GJ. London: WB Saunders Company Limited, 1995: 238-242

3. Goldsmith WT, Friend KA, McKinney WG, Reynolds JS, Frazer DG, Smith J. An improved system for measuring breath and cough sounds [Abstract]. In: *Proceedings of the 24th International Lung Sounds Conference*. Marburg, Germany: International Lung Sound Associations, 1999: 35

4. Reynolds JS, McKinney WG, Goldsmith WT, Frazer DG. A system for reconstruction of cough sounds and components of cough sounds [Abstract]. In: *Proceedings of the 24th International Lung Sounds Conference*. 1999: 37

5. Friend KA, Goldsmith WT, Reynolds JS, Frazer DG. Acoustic tube reconstruction for the characterization of cough sounds. In: *Proceedings of the First Joint BMES/EMBS Conference.* 1999: 1017

6. Goldsmith WT, Reynolds JS, McKinney WG, Friend KA, Shahan D, Frazer DG. A system for recording high fidelity cough sound measurements. In: He B, Yana K, Cerutti S, eds,. *Proceedings of the 3rd International Workshop on Biosignal Interpretationl*. 1999: 178-181

7. Goldsmith WT, Reynolds JS, McKinney WG, Friend KA, Stolarik BM, Frazer DG. Mouth flow estimation during cough sound measurements [Abstract]. In: *Proceedings of the 19th Southern Biomedical Engineering Conference.* 2000: 78

8. Rosenberry K, Goldsmith WT, Reynolds JS, McKinney W, Frazer DG. Gender differences in voluntary cough sound spectra demonstrated by an inverse power law analysis [Abstract]. In: *Proceedings of the Second Joint BMES/EMBS Conference*. IEEE. 2002: 139

9. Colerridge JCG, Coleridge HM. Afferent vagal c-fibre innervation of the lungs and airways and its functional significance. *Rev Physiol Biochem Pharmacol.* 1984; 99: 1-110

10. Collier JG, Fuller RW. Capsaicin induced inhalation in man and the effect of disodium cromoglycate. *Br J Pharmacol* 1984; 81: 113-117

11. Shannon R, Baekey DM, Morris KF, Lindsey BG. Brainstem respiratory networks and cough. *Pulm Pharmacol* 1996; 9: 343-347

12. Jordan D. Central nervous mechanisms in cough. *Pulm Pharmacol* 1972; 22: 634-643

13. van Lunteren E. Daniel R, Deal EC Jr, Haxhiu MA. Role of costal and crural diaphragm and parasternal intercostals during coughing in cats. *J Appl Physiol* 1989; 66: 135-141

14. Wallois F, Macron JM. Nasal air puff stimulations and laryngeal, thoracic and abdominal muscle activities. Respir Physiol 1994; 97: 47-62

15. van Lunteren E, Haxhiu MA, Cherniack NS, Arnold JS. Role of triangularis sterni during coughing and sneezing in dogs. *J Appl Physiol* 1988; 65: 2440-2445.

16. Frazer D, Stolarik B, McKinney W, Stone S, Afshari A, Goldsmith T, Barkley J, Reynolds J, Weber K. Differences in airflow patterns during voluntary coughs that result from obstructive lung disease [Abstract]. *Biomed Eng: Recent Developments* 2002: 317-318

17. Friend KA, Goldsmith WT, McKinney WG, Watkins SA, Frazer DG, Salahuddin N, Petsonk EL, Abrons H. Wavelet analysis for the detection of wheeze in cough sounds. In: He B, Yana K, Cerutti S, eds. *Proceedings of the 3rd International Workshop on Biosignal Interpretationl.* 1999: 326-329

18. Rabiner, L.R. and Schafer R.W. *Digital Processing of Speech Signals.* Prentice Hall Inc., Upper Saddle River, New Jersey 1978

19. Van Hirtum, A, Berckmans D, Demuynck K, Van Compernolle D. Autoregressive acoustical modeling of free field cough sound. *IEEE* 09/02: 493-495

20. Castranova V, Frazer DG, Manly LK, Dey RD. Pulmonary Alterations associated with inhalation of occupational and environmental irritants. *International Immunopharmacology 2* 2002: 163-172

21. Laude EA, Higgins KS, Morice AH. A comparative Study of the Effects of Citric Acid, Capsaicin and Resiniferatoxin on the Cough Challenge in Guniea pig and Man. *Pulmonary Pharmacology*. 1993; 6, 171-175

22. Tartar M, Pecova R, Karcolova D. Sensitivity of cough reflex in awake guine-pigs, rats, and rabbits. Bratisl. Lek. Listy. 1997; 10: 539-543

23. Tartar, Kacolova D, Pecova R, Brozmanova M. The Role of partial laryngeal denervation on the cough reflex in awake guinea-pigs, rats and rabbits. *Pulmonary Pharmacology*. 1996; 9: 371-372

24. Forsberg K, Karlsson JA, Theodorsson E, Lundberg JM, Persson CGA. Cough and bronchoconstriction mediated by capsaicin-sensitive sensory neurons in the guinea-pig. *Pulmonary Pharmacology*. 1988; 1: 33-39

25. Sheppard D, Rizk NW, Boushey HA, Bethel RA. Mechanism of cough and bronchoconstriction induced by distilled water aerosol. *Am Rev Respir Dis*. 1983; 127: 691-694

26. Clay TP, Thompson MA. Irritant induced cough as a model of intrapulmonary airway reactivity. *Lung 1985*; 163: 183-191

27. Allott CP, Evans DP, Marshall PW. A model of irritant-induced bronchoconstriction in the spontaneously breathing guinea-pig. *Br J Pharmacol* 1980; 71: 165-168

28. Braman SS, Corrao WM. Chronic cough. *Prim Care* 1985; 12: 217-25

29. Corrao WM. Chronic cough: an approach to management. *Compr Ther* 1986;12:14-19

30 Alarie Y, Nielsen GD, Schaper MM. Animal bioassays for evaluation of indorr air quality. In: Spengler JD, Samet JM, McCarthy JF, editors. *Indoor air quality handbook.* New York: McGraw-Hill; 2001 p. 23.1-23.49

31 Finger TE, Jeor VLS, Kinnamon JC, Silver WL. Ultrastructure of substance P- and CGRP-immunoreactive nerve fibers in the nasal epithelium of rodents. *J Comp Neurol* 1990; 294:293-305.

32 Grunditz T, Uddman R, Sundler F. Origin and peptide content of nerve fibers in the nasal mucosa of rats. *Anat Embryol* 1994; 189: 327-337

33 Karlsson JA, Choudry NB, Zackrisson C, Fuller RW. A comparison of the effect of inhaled diurectics on airway reflexes in humans and guinea pigs. *Journal of Applied Physiology* 1992; 72: 434-438

34 Bergen DR, Sampson SR. Characterization of intrapulmonary, rapidly adapting receptors of guinea pigs. *Respiratory Physiology* 1982; 47: 83-95

35 Sommer B, Montano LM, Chavez J, Gustin P, Vargas MH. Guinea pig lung resistance shows circadian rhythmicity not influenced by ozone. *Respiration Physiology*. 1998; 113: 223-229

36 Randall BR. *Frequency Analysis.* Denmark: K. Larsen and Son; 1987: 19-49

37 Beranek BL. *Acoustics*. New York: McGraw-Hill Book Co; 1954: 333-334

38 Proakis JG, Dimitrix MG. *Digital Signal Processing*. New Jersey: Prentice Hall; 1996: 49, 400-403, 917, 925-929

39 Agrawal KP. Specific airway conductance in guinea pigs: normal values and histamine induced fall. *Respiratory Phsyiology*. 1981; 43: 23-30

40 Porges G. *Applied Acoustics*. New York: John Wiley and Sons; 1997: 17-18

41 Pennock BE, Cox CP, Rogers RM, Cain WA, and Wells JH. A non-invasive technique for measurement of changes in specific airway resistance. *Journal of Applied Phsyiology*. 1979; 46:399

42 Shlens, Jon. A Tutorial on Principal Component Analysis. 2003. Salk Institute for Biological Studies. 25 March 2003 <http://www.snl.salk.edu/~shlens/pub/notes/pca.pdf>